DEVICE PHYSICS OF THIN-FILM POLYCRYSTALLINE CELLS AND MODULES

Final Report

September 2001 - October 2004

by

James R. Sites
Department of Physics
Colorado State University
Fort Collins, Colorado 80523

Work performed under Subcontract ADJ-1-30630-06
National Renewable Energy Laboratory
1617 Cole Boulevard
Golden, Colorado 80401

SUMMARY

Work has been performed at Colorado State University on basic measurements of CIGS and CdTe solar cells fabricated at a number of collaborating laboratories. The goal has been to explain several features seen in these measurements and quantitatively assess their impact on device performance.

The first area of study has been whole-cell analysis. Individual projects have included development of more effective separation of losses, the role of copper incorporation and migration with CdTe cells, the current-voltage consequences of the conduction-band offset in CdS/CIGS cells, alternative buffers for CIGS cells, and the development of the CurVA software for analysis of current-voltage curves.

The second area of study has been the use of a highly focused light spot (LBIC) to investigate spatial variations in polycrystalline solar cells. The local effects of elevated-temperature stress on CdTe cells has received the most attention, but we have also demonstrated that LBIC can be combined with other non-uniformity studies on the same cell and that it is possible to partially construct the J-V curve at individual local positions.

The third task has been the study of defect-states. With CIGS cells, we used low-temperature capacitance measurements to compare absorbers fabricated by evaporation with those made by selenization and to compare CdS buffer layers with the Cd-partial-electrolyte. For CdTe, photoluminescence from single crystals with controlled introduction of copper and oxygen has been compared with that from solar-cell material.

The final task area has been numerical simulation. We have defined and advocated a set of baseline parameters for CIGS and CdTe cells. Specific projects have included explanations of apparent quantum- and collection-efficiency effects, the impact of conduction-band offset on current-voltage curves, the effects of absorber grading in CIGS cells, and the 2-D analysis of grain-boundary effects.

TABLE OF CONTENTS

FIGURES

1. INTRODUCTION

The objectives of the Colorado State University program have been to (1) quantitatively separate individual performance-loss mechanisms in CIGS and CdTe solar cells using existing experimental and analytical techniques, (2) expand the tool set for such measurement and analysis and (3) suggest fabrication approaches or modifications to minimize the losses. The work performed during the past three years is described in this report or in the publications referenced in the final section. Detailed information can also be found on our website: www.physics.colostate.edu/groups/photovoltaic.

The experimental and analytical work in this report has largely been done by a dedicated group of graduate students. Pamela Johnson compared the defects in CIGS cells made with different absorbers and buffer strategies. Alex Pudov coordinated a study of CdTe cells made with varying amounts of copper in the back contact. More recently, he and Ana Kanevce have analyzed J-V distortions in CIGS cells with varying Ga content and CdS properties. Markus Gloeckler has used numerical simulation to explain non-superposition and voltage limitations in CIGS cells, apparent quantum-efficiency results in CdTe, collection-efficiency effects, and consequences of absorber grading. Caroline Corwine has studied the PL signatures of Cu impurities in crystalline and polycrystalline CdTe. Samuel Demtsu has coordinated CdTe elevated-temperature stress studies and loss analysis. Tim Nagle and Alan Davies have done LBIC analysis of both CdTe and CIGS cells with particular emphasis on non-uniformities related to stress. Jun Pan, with Alan Fahrenbruch, has explored the consequences of thinning the CdTe absorber.

Prof. Sites' group has actively participated in the NREL-sponsored National CdTe and CIS R&D Teams. It has had productive collaborations with Prof. Sampath's group at Colorado State, as well as with researchers at Aoyama Gakuin University, Colorado School of Mines, First Solar Inc., Global Solar Energy, IEC University of Delaware, ISET, Moldova State University, NREL, Shell Solar Industries, University of Illinois, University of Oregon, University of South Florida, and University of Toledo.

2. WHOLE-CELL LOSS ANALYSIS

The long-term strength of the Colorado State photovoltaic program has been the characterization and analysis of thin-film polycrystalline cells. Generally, the approach has been a combination of careful measurement of and quantitative separation of the various loss mechanisms. During the past three years, the basic cell-measurement equipment has been upgraded in several ways. First, a commercial solar simulator has become the primary light source for J-V measurements. Its optics and light path were adjusted after delivery to insure uniform standard intensity over the beam area. Second, modular cell-mounts have allowed measurements over time and transfer between measurement stations without movement of the contact probes. Third, the calibration procedure and the temperature control have been made more user-friendly so that the number of cells that can be reliably measured in a day, including their temperature variations, has been significantly increased.

2.1. CdTe Loss Analysis. The traditional parametrization of CdTe J-V curves in terms of their current, voltage, and fill-factor was extended to identify and quantify the individual losses that determine the three basic parameters. The goal was that each mechanism be assigned a clear physical interpretation, that can be straightforwardly measured, and that has a well-defined numerical impact on cell efficiency. Such parameters, sometimes referred to as "third-level metrics", are used to separate the individual CdTe loss mechanisms so that one identifies the larger losses and hence the larger possibilities for cell improvement. The same general strategy applies to loss analysis of CIGS [1] and other solar cells.

For illustrative purposes, we chose two very different CdTe cells: a typical production cell (9.6% efficiency) from First Solar, LLC, and the record CdTe cell (16.5%) made at NREL [2]. The current-voltage (J-V) curves for these two cells are shown in Fig. 2-1, and their quantum-efficiency (QE) curves in Fig. 2-2. For comparison, we also show curves for what we believe is a realistic target cell (19%) for CdTe and an ideal cell with the CdTe band gap (30%).

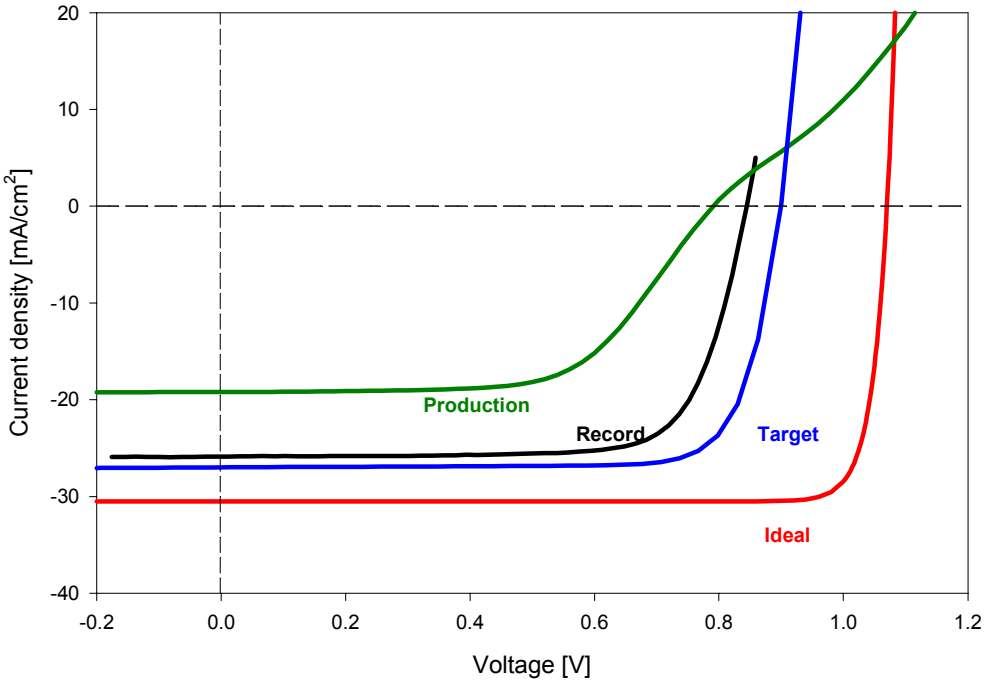

Figure 2-1. CdTe J-V curves for First Solar production cell, NREL record cell, target cell, and ideal cell.

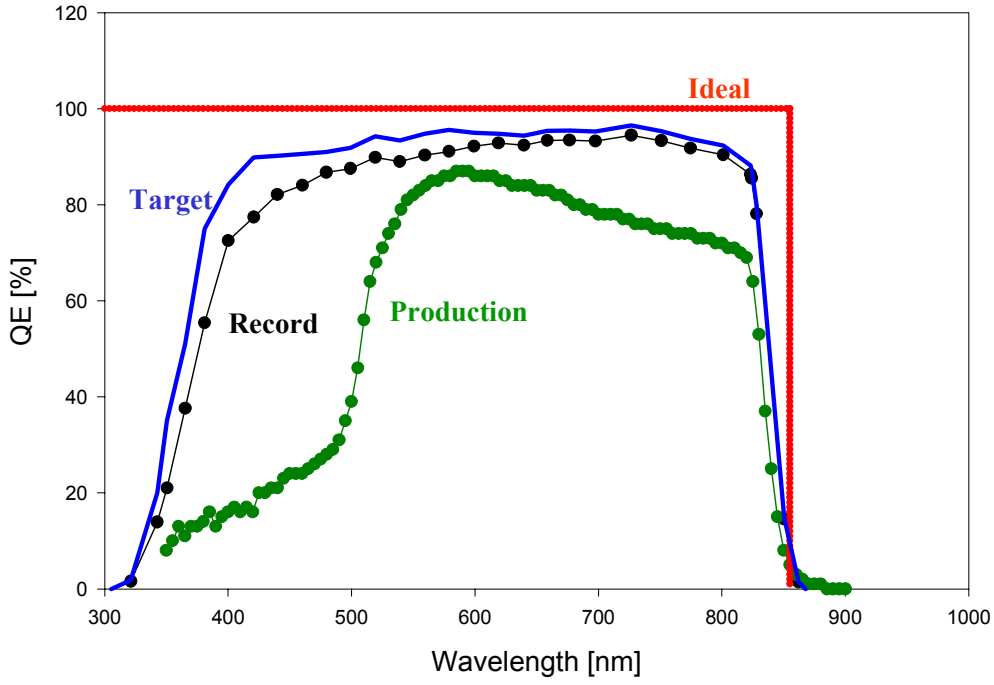

Figure 2-2. QE curves for same CdTe cells as Fig. 1.

The J-V and QE curves of these cells, as well as optical data from the window layers, were then used to deduce the following individual losses:

Voltage Losses
- Carrier Density/Built-in Potential
- Recombination Velocity

Current Losses:
- Reflection
- Glass Absorption
- TCO Absorption
- CdS Absorption
- Absorption by Mixed CdS/CdTe Layer
- Deep-Penetration Collection Loss

Fill-Factor Losses
- Series Resistance
- Leakage Conductance
- Direct Effect of Low V_{OC}
- Diode Quality Factor
- Back Contact
- Voltage Dependence of J_L

The individual current losses and the first three fill-factor losses can be accurately accessed. The other losses are less accurate and can require judgment in interpretation.

Figure 2-3 shows the strategy for quantifying the current losses for the record CdTe cell. Through QE and optical measurements, the fraction of photons for each wavelength that are collected or are lost to each of the various mechanisms is determined. The spectrum of lost photons for one of these mechanisms can then be multiplied by the photon-current spectrum and the product integrated over wavelength up to the band-gap cutoff [3]. The loss for each such region is shown in Fig. 2-3, and collectively these losses account for the difference between the actual short-circuit current and the maximum current possible for the band gap and spectrum used.

The voltage and fill-factor breakdowns for this record-efficiency cell are nearly as straightforward, but there can be complications when the cells are further from ideal, i.e. when the J-V curve is distorted by the back contact barrier or when the cell response is not spatially uniform. Even when such complications make the individual loss values less certain, the tracking of the parameters with fabrication changes or post-fabrication stress is a valuable tool for tracking the physical mechanisms responsible. Samuel Demtsu will give a talk on this project at the 31st PVSC in January.

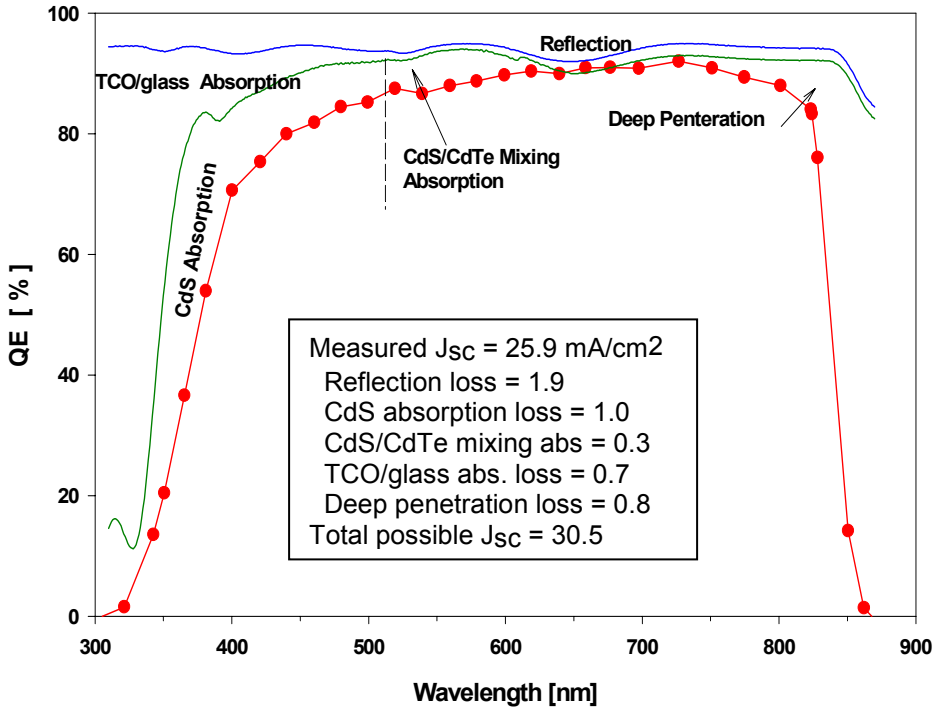

Figure 2-3. Separation of current losses in record CdTe cell.

2.2. Copper Migration in CdTe Cells. In collaboration with W. Sampath's group at CSU and several other colleagues, we have explored the role of copper in the formation of the back contact in CdTe cells. Our proposed model is shown in Fig. 2-4. In the absence of copper, there is a significant hole barrier at the back of the CdTe layer. In the schematic shown, there is also an overlap between the front and back barriers that has the effect of lowering the conduction-band maximum and hence limiting the voltage. As copper is added, it progressively dopes the CdTe more p-type or forms a distinct Cu-Te layer. In either case, the result is a lower and narrower barrier.

The copper, however, can migrate away from the high concentration region, effectively reversing the barrier reduction and most likely accumulating in the CdS. The rate of the copper migration will be higher at elevated temperature, but is also affected by the electric field within the CdTe. In particular, there is a relatively large internal field for the zero-bias diagram shown, which retards the migration of positive copper ions. At open-circuit voltage, however, the field is considerably reduced, and one would expect the larger rate of migration.

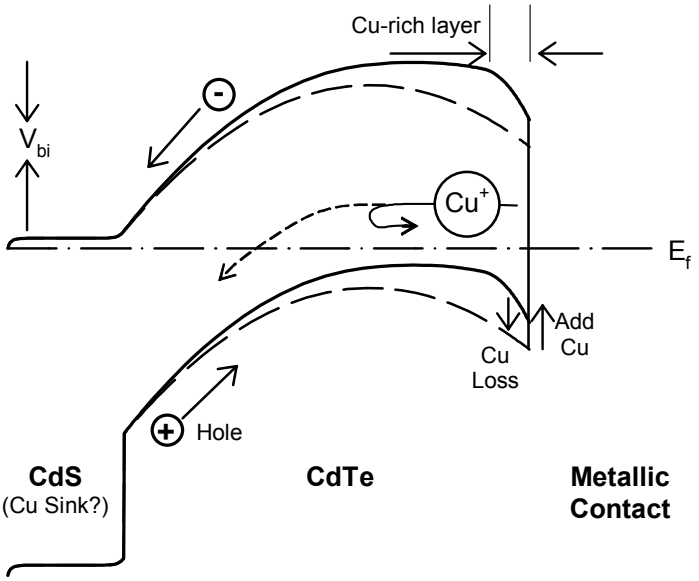

Figure 2-4. Proposed CdTe band picture for Cu addition and migration.

To test the model depicted in Fig. 2-4, we measured samples made by Sampath's group with a range of copper (0, ¼, ½, 1, and 2 times the usual amount) in the formation of the back contact. The J-V curves for this set of samples are shown in the left part of Fig. 2-5. Without intentional copper, the fill-factor was significantly reduced, and the back barrier also limited the current above V_{OC}. There were progressive improvements in fill-factor up to the standard copper amount, but additional copper made little difference.

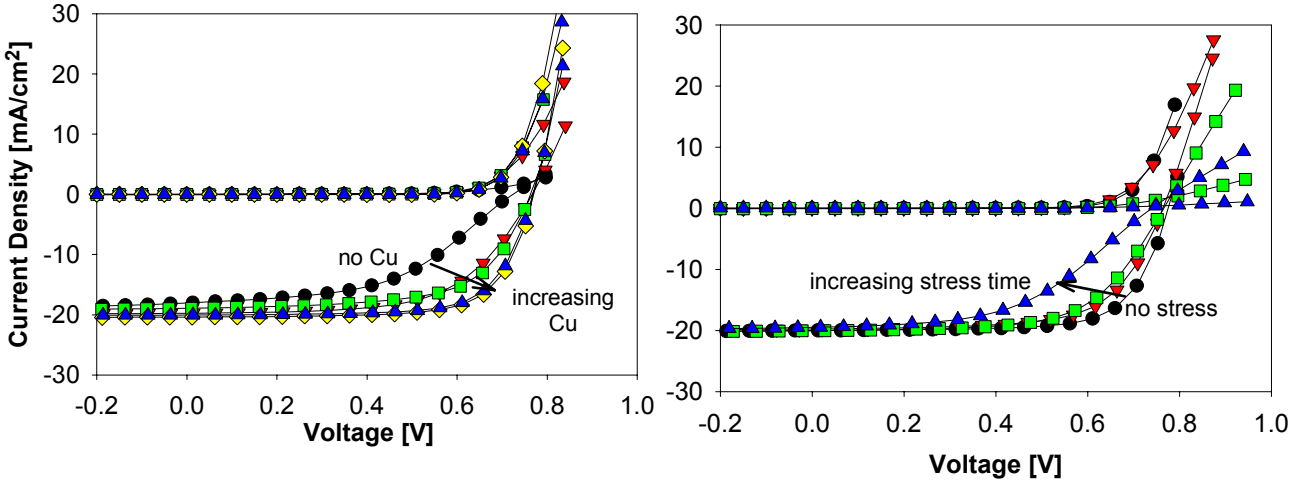

Figure 2-5. As-deposited CdTe J-V curves with varying back-contact copper (left). Reverse effect when standard-copper cell is stressed (right).

This situation was reversed (Fig. 2-5, right) when a cell with the standard amount of copper was stressed under illumination at short-circuit and elevated temperature (100°C) for increasing lengths of time. Hence the interpretation (Fig. 2-4) that copper during deposition reduces the barrier, but out-migration under stress restores it.

Another result that supported the Fig. 2-4 model was a progressive change in capacitance as the copper content was increased, coupled with a reversal of this change as a standard cell is stressed. Still more evidence, discussed in the following section, was the good spatial uniformity in cell response when a cell had sufficient copper, but the similar degradations in uniformity when the amount of copper was initially insufficient or was subsequently reduced by stress. This study, which involved Caroline Corwine, Alex Pudov, Markus Gloeckler, and Samuel Demtsu, was presented at the 2003 NCPV Review and later published in Solar Energy Mat. and Solar Cells **82**, 481-489 (2004).

2.3. CdS/CIGS Conduction-Band Offset. The conduction-band offset between CdS and CIGS varies as the gap of CIGS is increased (Fig. 2-6). Since most of the band-offset shift occurs in the conduction-band between CdS and CIGS [4], there is a progression from a positive offset (also referred to as Type I, or a "spike") to a negative offset (Type II, or "cliff") that tracks the increasing band gap. The transition from positive to negative occurs near x = 0.5, which corresponds to a band gap near 1.35 eV. One effect of the CdS/CIGS conduction-band offset is the failure of light/dark superposition in the current-voltage curves. Fig. 2-7 shows light and dark J-V data from a good-quality CIGS cell made at the Institute of Energy Conversion. Three different temperatures are shown, and apart from the lack of light/dark superposition, the curves are well behaved. The temperature dependence of the light curves, as expected, is about –1.9 mV/K. The temperature dependence of the dark curves, however, is –3.3 mV/K, which implies a V_{OC} that becomes implausibly large at lower temperatures.

The data in Fig. 2-7 was explained through a combination of the CdS/CIGS conduction-band offset that is harder for electrons to surmount at lower temperature, photogeneration in the CdS, and significant CdS trap densities. Numerical simulations, as described in Section 5, gave a good quantitative fit to the data in Fig. 2-7. Parameters

such as the TCO/CdS band offset and the specific carrier and trap densities also affect the simulation results, but are not central to the superposition failure [M. Gloeckler, C.R. Jenkins, and J.R. Sites, "Explanation of Light/Dark Superposition Failure in CIGS Solar Cells," Proc. Mat. Res. Soc **763**, 231-236 (2003)].

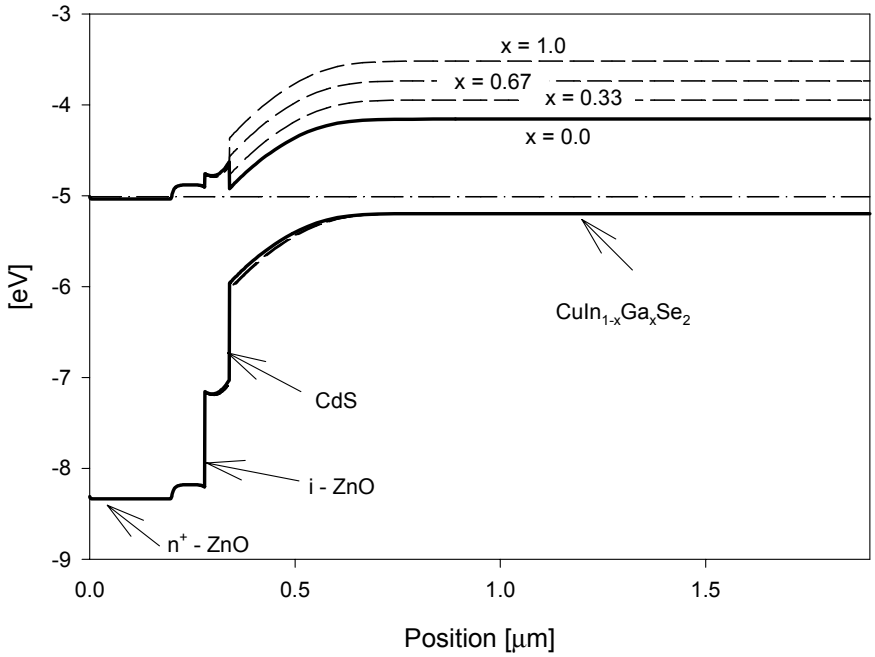

Figure 2-6. Band structure of CIGS cell as absorber is varied from CIS to CGS.

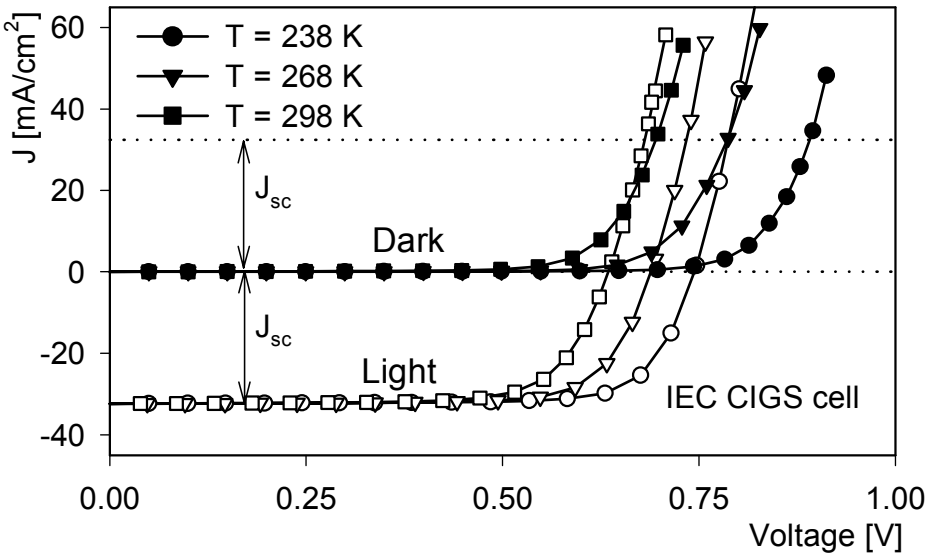

Figure 2-7: Light/dark J-V crossover in CIGS cell at three temperatures.

In the extreme case, the conduction-band offset distorts the light curves as well as the dark. An intermediate case, where the blue photons are suppressed, can produce a distorted J-V curve, which is referred to as the "red kink" [5,6]. Alex Pudov and Ana Kanevce have done extensive comparison of the white-light, red-light (no photons below 600 nm), and dark curves from CdS/$CuIn_{1-x}Ga_xSe_2$ cells fabricated by Falah Hasoon and Hamda Al-Thani of NREL. These absorbers were deposited by co-evaporation to produce a spatially uniform band gap. The standard CdS thickness was approximately 50 nm, and the cells were completed with the typical ZnO bi-layer.

The current-voltage curves from a series of such CIGS cells made with increasing Ga-concentration, and hence increasing band gap, are shown in Fig. 2-8. Without Ga, the conduction-band offset is largest, and there is a slight distortion of the white-light curve. The red-light curve, however, is much more distorted and shows the characteristic red-kink shape. In reverse bias, its photocurrent magnitude is lower due to filtering of the illumination source, but is otherwise well behaved. There is a transition near zero bias, and in forward bias the red curve merges with the dark curve. As the band-gap is increased in Fig. 2-8, the conduction-band offset is reduced, the red-kink disappears near a gap of 1.2 eV, and superposition between light and dark curves is restored.

Since thicker CdS is expected to produce a larger red-kink distortion [6], we also measured cells fabricated with different CdS thicknesses on both co-evaporated and three-stage [7] CIS absorbers. The specific CdS thicknesses were determined by comparison of the integrated short-wavelength currents to those of cells with known CdS thicknesses [8]. The white-light curves shown in Fig. 2-9 were similar for all CdS thicknesses with each absorber type. The red-curve progressions, however, show increasing distortions with increasing CdS thickness. Specifically, the single-stage cells with 20-nm and 50-nm CdS were well-behaved, but the thickest-CdS (80-nm) cell showed a considerable distortion. Three-stage-absorber cells were similar: the cell with 15-nm CdS showed no distortion, and the cells with 50-nm and 80-nm CdS cells showed increasing amounts of distortion. The cells were also annealed in air, and with both absorbers, the thinnest-CdS cells acquired small red distortions, while the distortions in the thicker-CdS cells became larger.

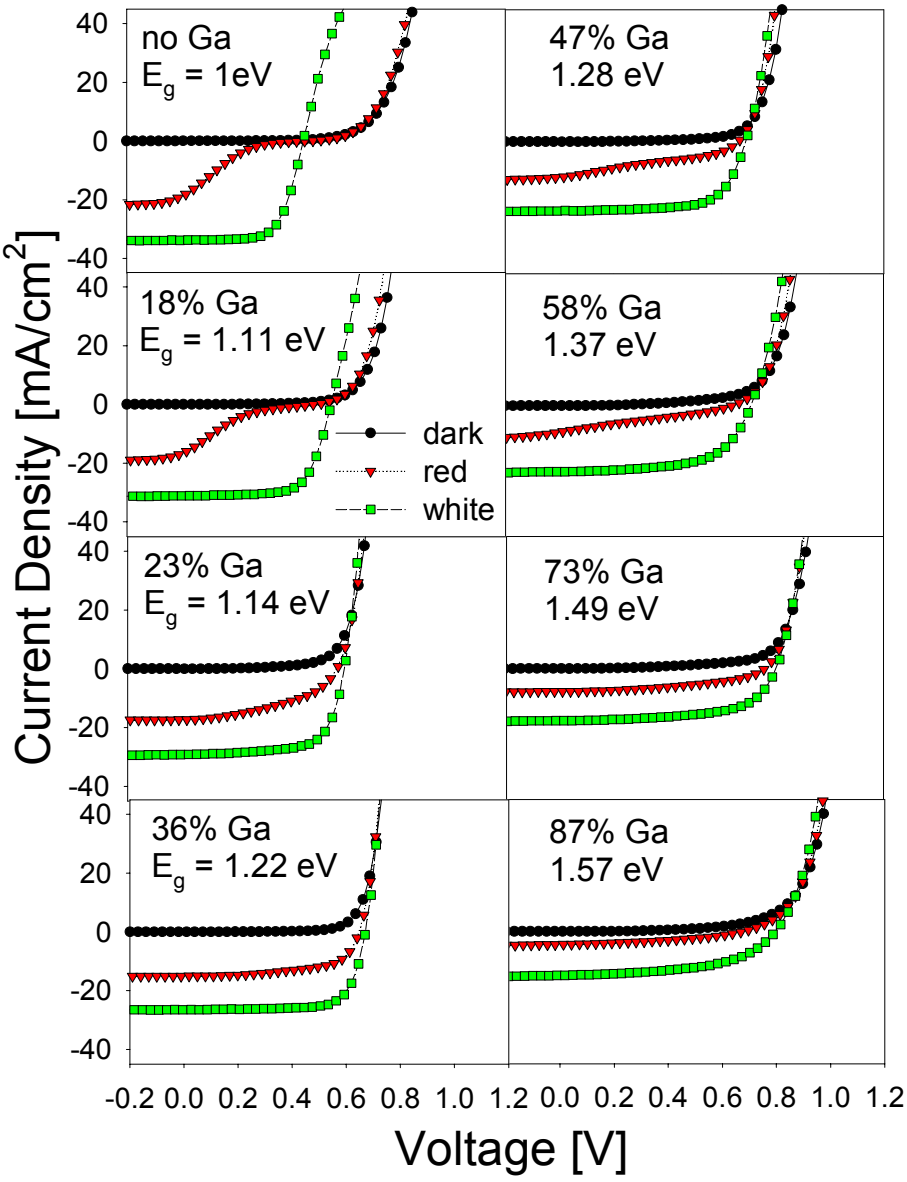

Figure 2-8. Experimental dark, red-light, and white-light J-V of the CIGS cells with variable Ga in the absorber.

Additional experiments showed that blue-light intensity as small as 1% of that normally found in sunlight was sufficient to remove most of the red kink. The time for white light to eliminate the kink was the order of one minute, while the time for restoration of the kink in the absence of white light was the order of one day. A

manuscript "Secondary Barriers in CdS/$CuIn_{1-x}Ga_xSe_2$ Solar Cells" has been submitted to the Journal of Applied Physics.

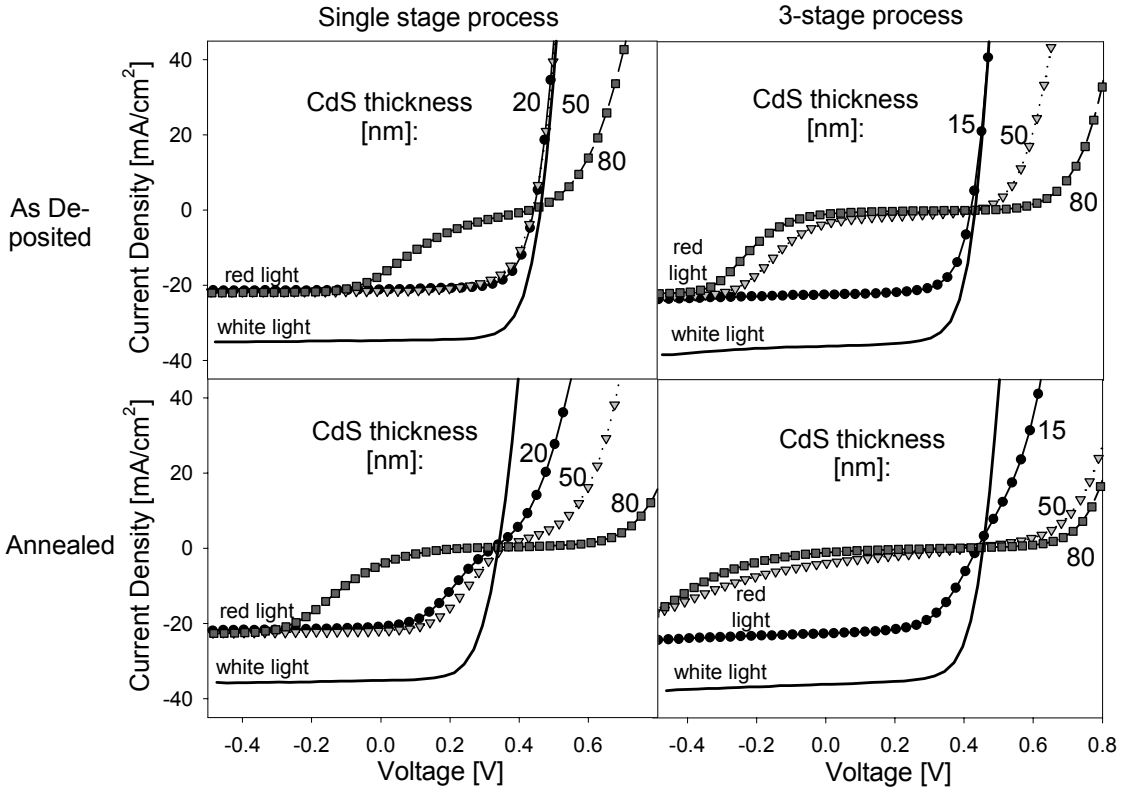

Figure 2-9. Experimental red- and white-light J-V from CdS/CIS cells of various CdS thickness for single- and three-stage CIS. With and without 200°C air-anneal.

2.4. CIGS with Alternative Buffers. A second collaboration, which has involved Alex Pudov at CSU, Miguel Contreras and Raghu Bhattacharya at NREL, Tokio Nakada in Japan, and Hans Schock in Germany, has explored alternatives to the CdS buffer commonly used with CIGS cells. One commonly realized advantage of wider band-gap buffers is an improvement in blue collection, as illustrated in Fig. 2-10. In this case, CdS and ZnS(O,OH) buffers were deposited by CBD onto nominally identical CIGS absorbers. The efficiencies were similar (19.2% and 18.6%), but clear differences were seen in QE. Even though the CdS cell had good short-wavelength collection, the higher band-gap buffer showed almost no loss between 400 and 700 nm. On the other hand, the CdS cell maintained better collection into the long-wavelength region and had a slightly

higher voltage. This work appears in the Proc. 3rd World Conf. on Photovoltaic Energy Conversion (Osaka), pp. 570-573 (2003).

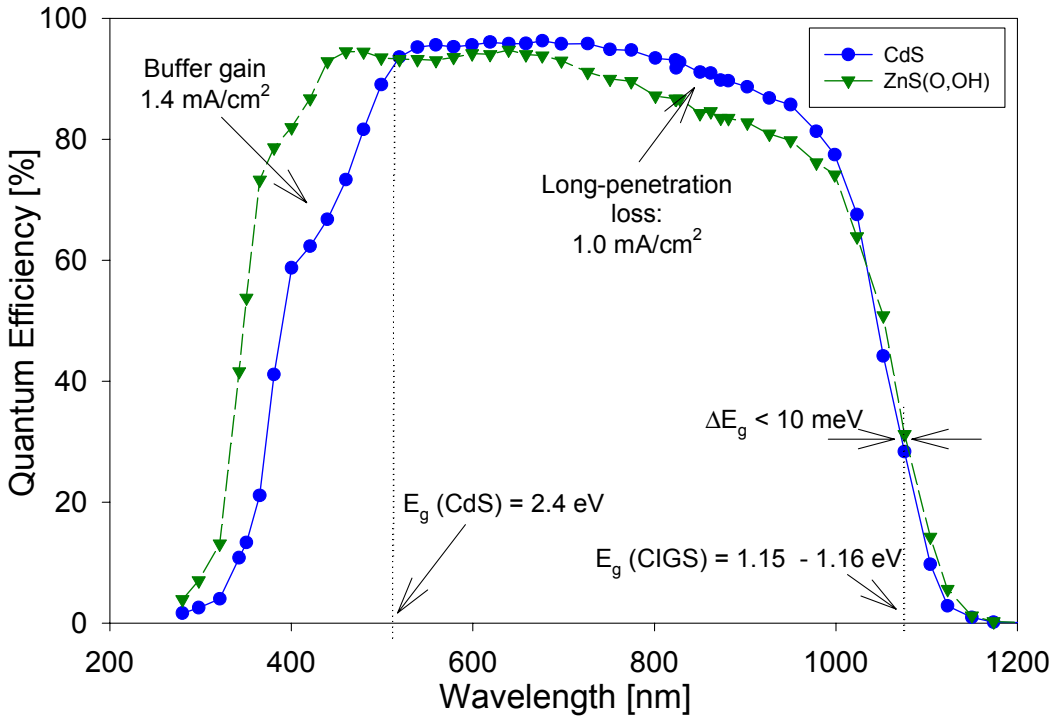

Figure 2-10. QE comparison of CIGS cells with CdS (19.2% efficiency) and ZnS(O,OH) (18.6%) buffer layers.

A larger band-gap buffer, however, means a larger conduction-band offset and thus the possibility of J-V distortions similar to those shown for CdS/CIS in Fig. 2-9. Such distortions are in fact seen, especially when red light is used. The current-voltage curves for three buffer layers, again deposited on nominally identical 1.15-eV CIGS absorbers, are shown in Fig. 2-11. CdS deposited at NREL yielded cells with very good superposition between dark, red-light, and white-light conditions. With ZnS(O,OH), deposited in Japan, the red curve was significantly distorted, the red and dark curves were artificially shifted to higher voltages for forward currents, and the white-light curve was very slightly distorted. With InS(O,OH), deposited in Germany, the pattern is similar, and the red-light distortion is somewhat larger. All the effects shown can be simulated in detail with a larger-than-optimal conduction-band offset. A manuscript containing this

work, “CIGS J-V Distortions in the Absence of Blue Photons,” has been accepted for publication in Thin Solid Films.

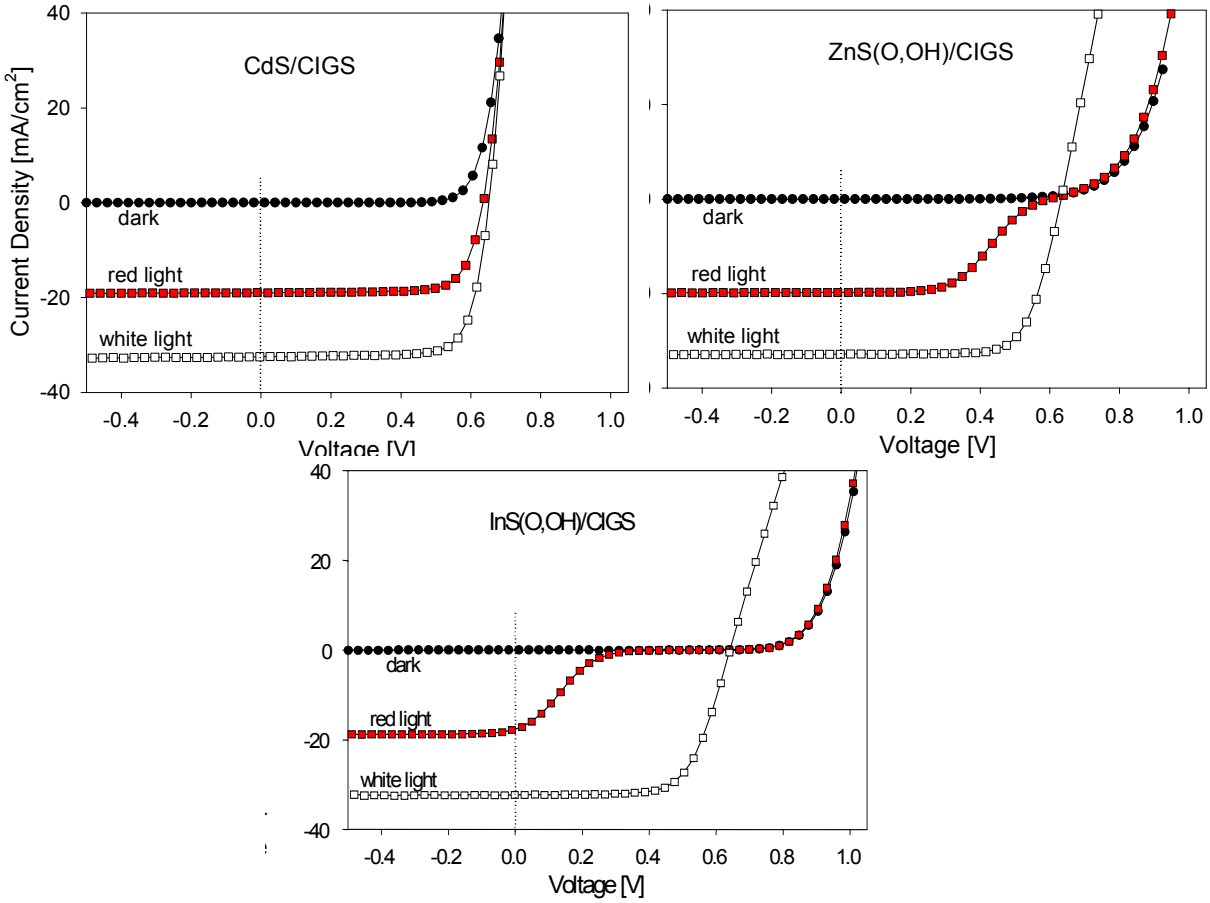

Figure 2-11. Dark, red, and white J-V curves for CIGS cells with three buffer layers.

2.5. CurVA Analysis Software. Markus Gloeckler has written a LabView software package to extract common parameters from experimental J-V data in a highly visual and interactive fashion. The idea of showing the same data in four formats was promoted by Jim Phillips of IEC and described in a recent review article by Hegedus and Shafarman [1]. What CurVA has added is the ability to use sliders to select the range of data to be fit (highlighted data points in Fig. 2-12). Hence one can exclude regions such as “rollover” and can vary the data range to instantly observe changes in the Fig. 2-12 fitting parameters. CurVA also allows the user to smooth the data by various amounts, again with a slider, and to see the fit superimposed on the data in each of the four formats. This

software is now being used routinely in our lab and by several researchers at NREL. It was specifically adapted to interact directly with the data base and measurement system in NREL's thin-film stability lab.

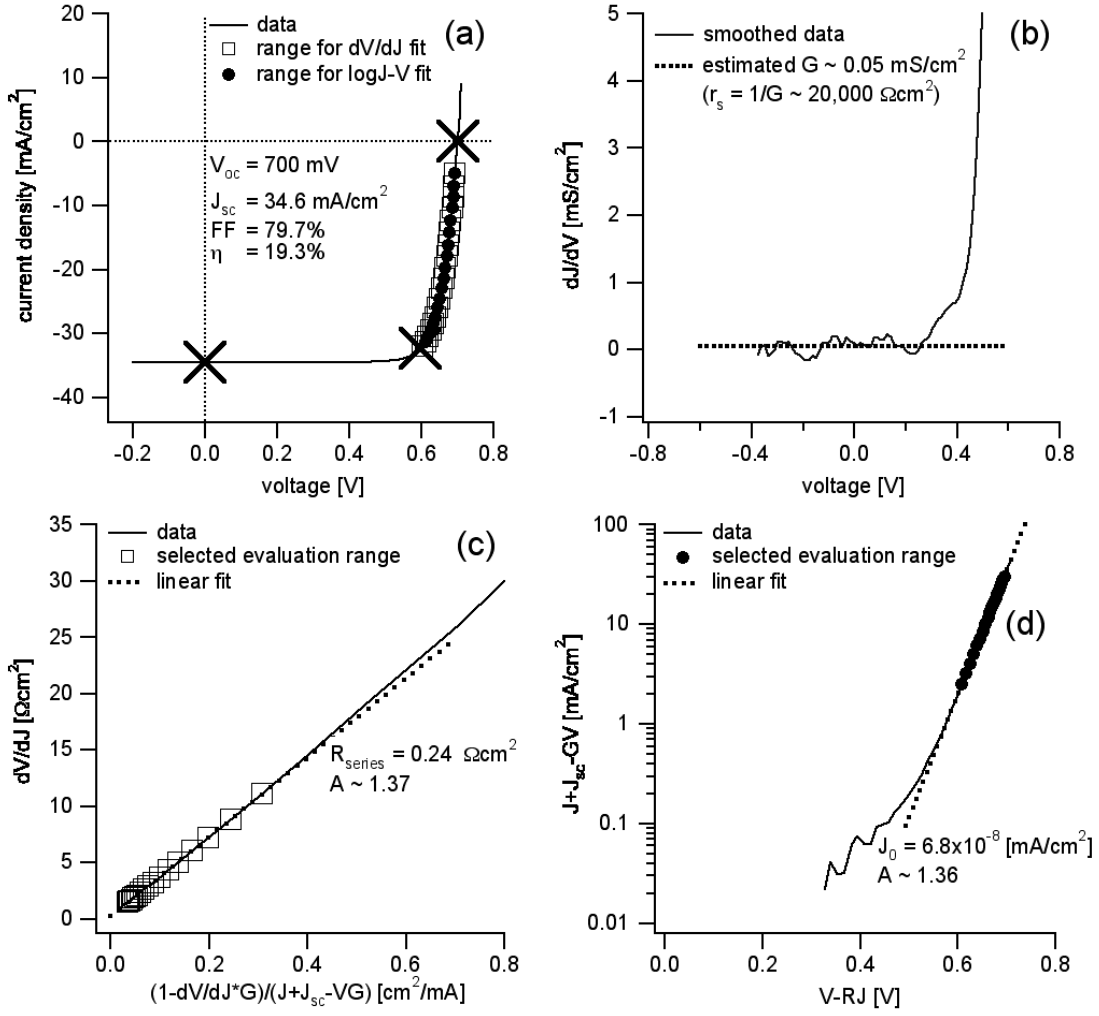

Figure 2-12. J-V data displayed by CurVA software in (a) linear format, (b) dJ/dV vs voltage format, (c) dV/dJ vs inverse current format, and (d) ln J vs V format.

3. SMALL-SPOT STUDIES

3.1. Light-Beam Induced Current (LBIC). Small light-spot measurements provide a direct link between the spatial non-uniformities inherent in thin-film polycrystalline solar cells and their overall performance. Our LBIC system [9,10] uses diode lasers with wavelengths in the visible and near infrared. The smallest spot size achieved is slightly under 1 micron, and the objective lens has a correction collar for focus through CdTe superstrates. Precision x- and y-axis translation stages allow photocurrent mapping. The photocurrent sensitivity is below 0.1 nA, which allows very good signal-to-noise at one sun intensity and one-micron spot-size. Reflection may be measured simultaneously.

Three standard resolutions are used: low (5-mm field with 100-µm spot), medium (500-µm field with 10-µm spot), or high (50-µm field with 1-µm spot). These resolutions are illustrated in Fig. 3-1 for a CIGS cell illuminated with a focused 638-nm laser beam that has intensity near one sun in each case. The QE scale is to the right. The low-resolution plot on the left shows approximately half the cell. The grid fingers have no response, and green over most of the area signifies relatively uniform QE between 80 and 82%. Blue towards the edge is slightly lower QE. The square in the left map is magnified 10 times (middle plot), and its square is magnified 10 more times (right). At high resolution, several low response areas, 2-5 µm in diameter, are observed.

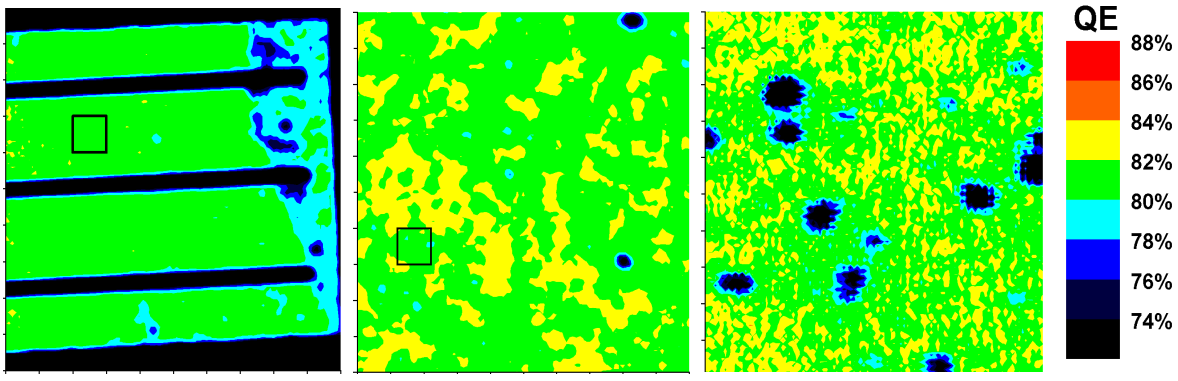

Figure 3-1. CIGS QE photomaps with 100-, 10-, and 1-µm beams.

Presentation of LBIC results can be done with QE photomaps, as shown in Fig. 3-1, or with histograms showing the distribution of QE response. The medium-resolution data from a CdTe cell is shown in both formats in Fig. 3-2. The photomap presentation is

useful for highlighting specific defects, such as the dark spot shown, and response to variations in voltage bias or illumination wavelength. The histogram format is more useful to illustrate overall photocurrent uniformity and how it might change with time.

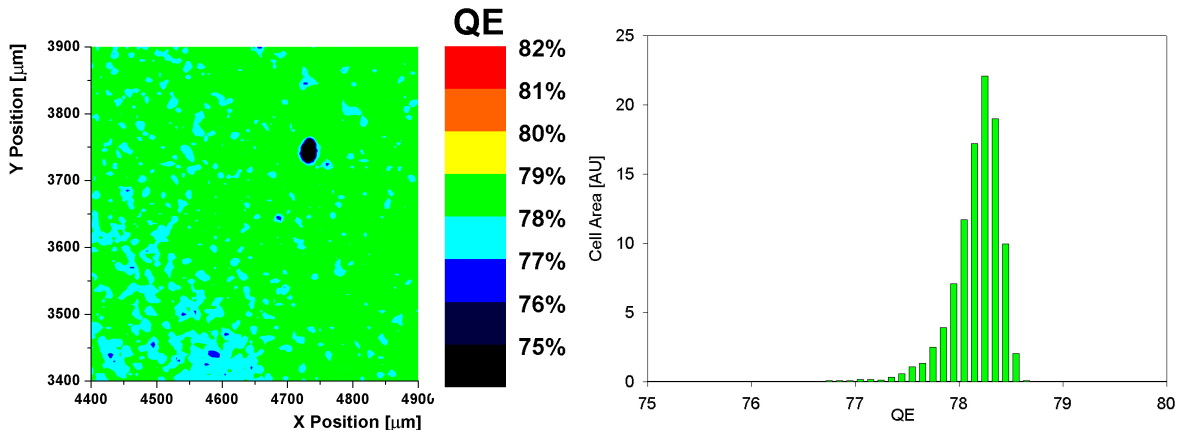

Figure 3-2. CdTe LBIC data expressed as QE map and as histogram.

The histogram format is used in Fig. 3-3 to show the difference between two otherwise identical CdTe cells with different back-contact processing. Both cells had very uniform QE initially. After exposure to elevated-temperature stress, the left-hand cell with standard back-contact processing showed only modest decrease in average QE and uniformity. The right-hand cell, however, was made with part of the contact procedure omitted, and it showed much larger reductions in both the QE magnitude and uniformity.

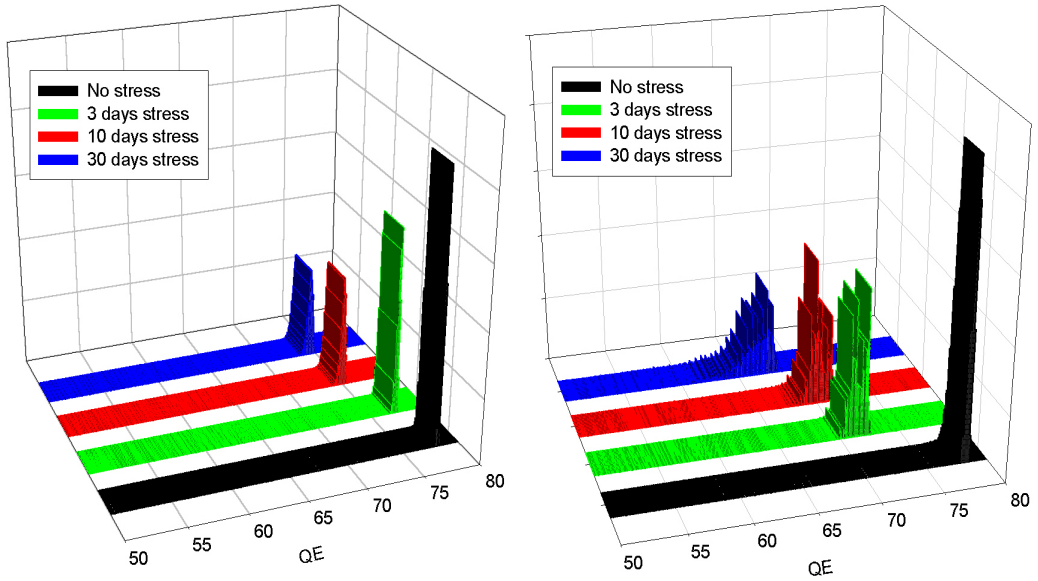

Figure 3-3. Contrasting QE histograms from two CdTe cells.

3.2. Types of LBIC Features. Several small-area reduced-QE features are seen in the high-resolution maps in Figs. 3-1 and in 3-2. These well-defined areas are dead spots a few microns in dimension that reduce cell current by a very small amount, but do not otherwise affect cell performance. They can result from either local optical defects or local contact flaws, and they occur with essentially all solar cells, including III-V cells that are space-qualified. A variation, shown in Fig. 3-4, is the existence of small reflective areas. The cell used for Fig. 3-4 is a silicon reference cell supplied by Astropower that was covered with many small (20 micron) reflective spots. In this case the QE decrease at such a spot was very nearly equal the increase in reflection.

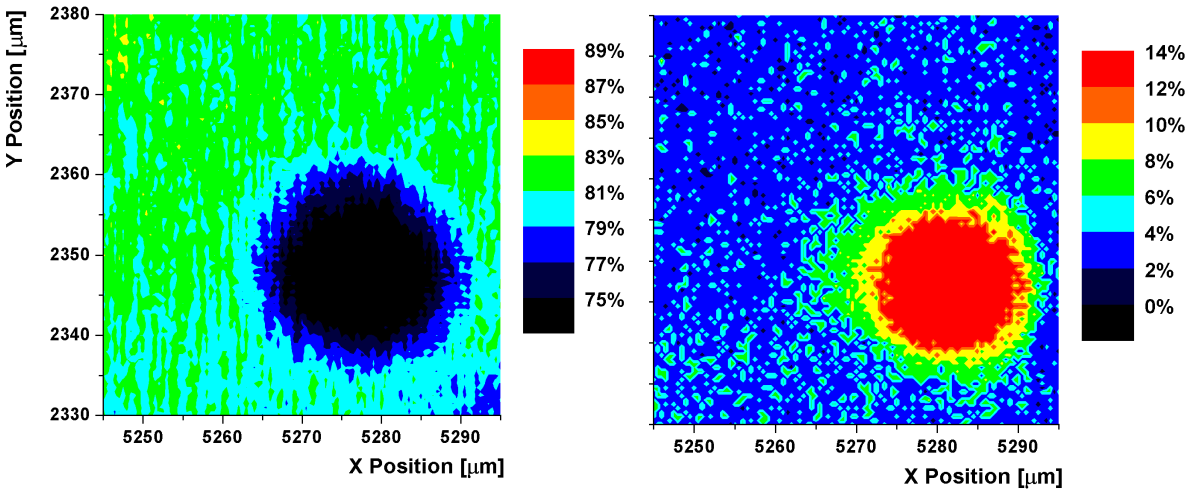

Figure 3-4. Quantum-efficiency map (left) and reflection map (right) from same area of a silicon solar cell.

A much more serious situation is illustrated in Fig. 3-5, where a grid finger on a CIGS cell was accidentally shunted at the cell edge. In this case, QE at the shunt was zero, that of a large surrounding area was very small, and the cell's J-V curve had a highly shunted signature. The initial QE map with the shunted contact is shown to the left. After the metallic shunt was dissolved with acetone, however, a uniformly high QE was restored, and the cell regained its normal J-V curve. This is an extreme example, and work to identify and analyze less catastrophic shunts is underway, but not completed. Part of the continuing work by Tim Nagle is to use the Pspice software to quantify the relationship between the contact–layer and shunt parameters and the corresponding QE maps.

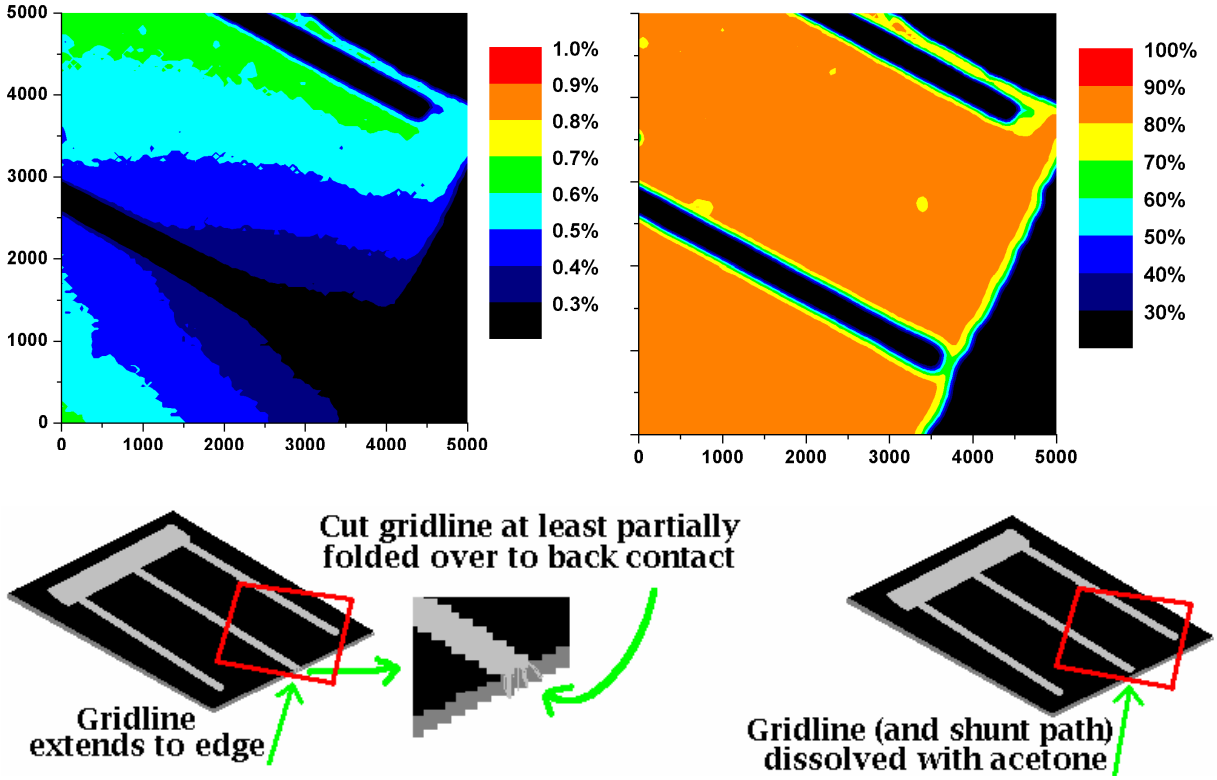

Figure 3-5. Massive reduction in CIGS QE near a complete short (left), and recovery after removal of the shunt (right).

A general objective for small-area analysis is to apply different non-uniformity techniques to the same solar cell. A joint effort between Tim Nagle and Scott Feldman at the Colorado School of Mines has been to correlate CSM electoluminescence (EL) mapping [11] of CdTe cells with our photocurrent maps. To date, they have collaborated on two different sets of CdTe cells, and also a high-efficiency III-V cell. One comparative example is shown in Fig. 3-6, which covers an entire 3-mm CdTe cell. Clearly the two techniques are seeing the same major features. These particular features were not deliberately introduced, but primarily resulted from multiple measurements using mechanical probes. Additional comparisons of smaller areas have consistently shown a strong correlation between the two techniques.

Other small-area measurements, such as thermography [12] and photoluminescence [13], have been developed by other groups, and it is now entirely practical to correlate experimental non-uniformities across a broad set of techniques. Registration to the same cell area has been straightforward, since there are usually easily identifiable features.

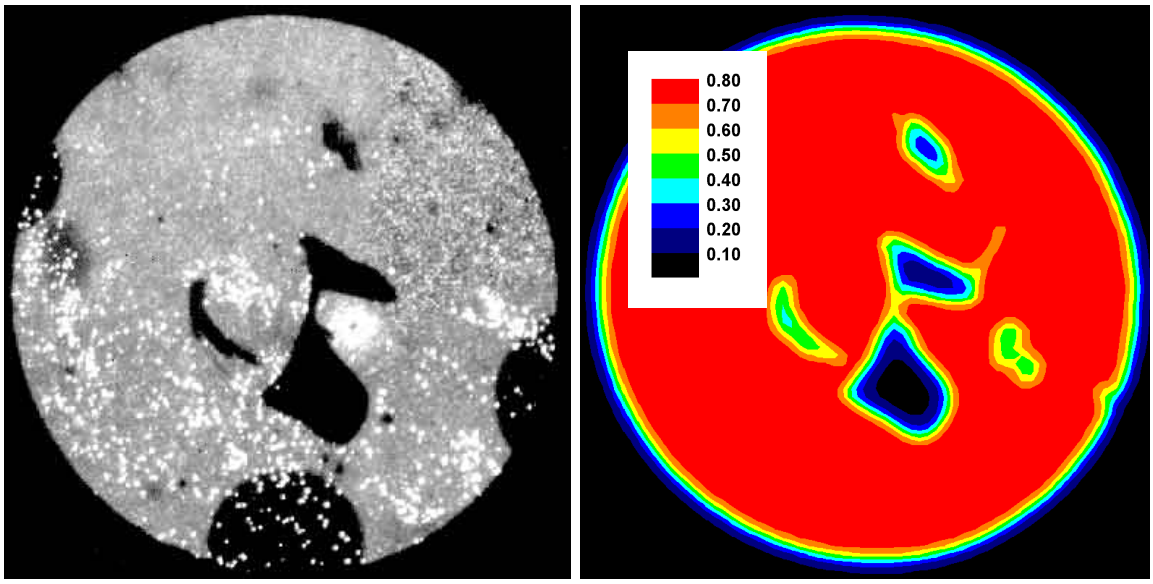

Figure 3-6. CSM scans of electroluminescence (left) and CSU scans of quantum efficiency (right) on same CdTe cell.

3.3. LBIC for Stress Studies. CdTe cells in particular can show performance degradation after exposure to elevated-temperature stress, and in almost all cases the changes do not occur uniformly. Figure 3-7 illustrates a typical situation in which a CdTe cell made by Sampath's group at Colorado State was stressed under illumination at 100°C and short-circuit. The average QE decreased by about 2%, but not uniformly over the cell area. In fact, a few small areas of significant reduction have started to appear.

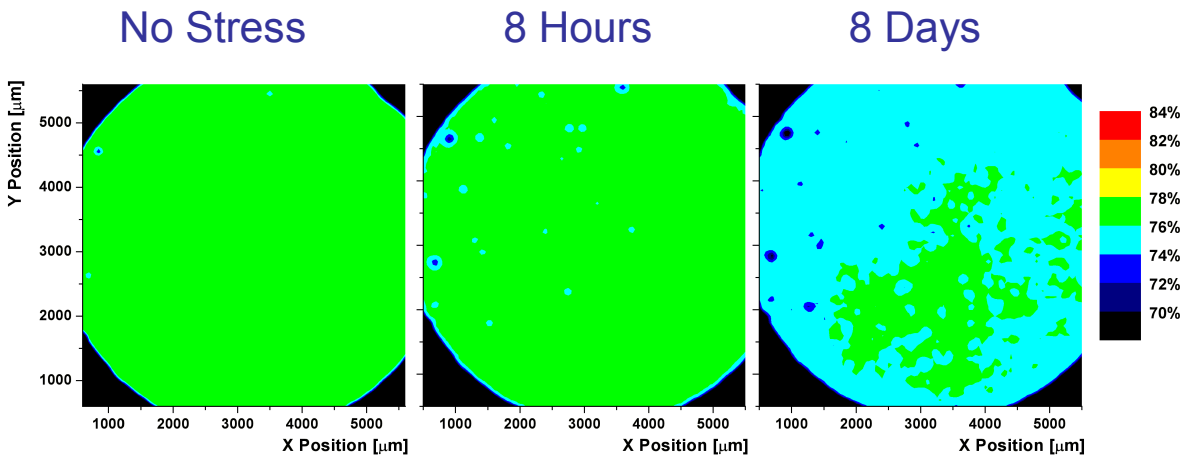

Figure 3-7. Changes in QE map of CdTe cell with stress.

The stress-induced changes shown in Fig. 3-7 are fairly modest, but in other cases, they can be significantly larger. Figure 3-8 shows a CdTe cell made at the University of South Florida before and after 5 days of stress under illumination at 90°C and zero bias. The row of dots near the top is due to repeated probe placement and is not related to the stress. In this case, there is a major QE reduction in one area of the cell, which is a less dramatic version of the shunt signature shown in Fig. 3-5.

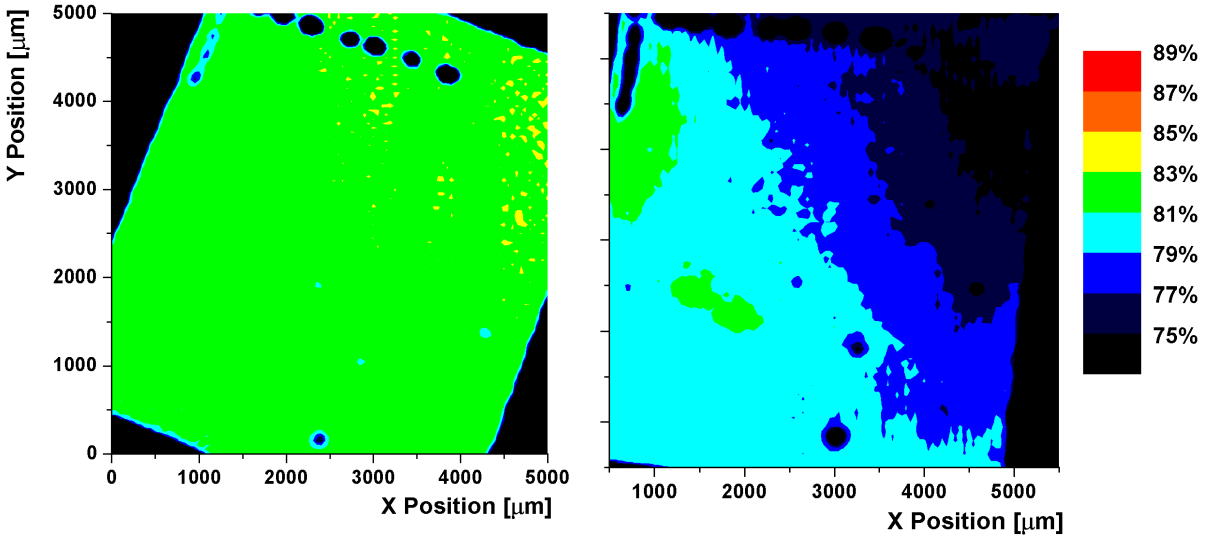

Figure 3-8. LBIC map of CdTe cell before (left) and after stress.

In other cases following similar exposure to stress, the QE drops essentially to zero over large, but delineated, areas of a CdTe cell. When this large dead-area scenario occurs, it strongly suggests a different problem, one in which the back contact is no longer effective over significant regions of the cell. This can occur even when there is no physical evidence of contact delamination.

3.4. Voltage Dependence of LBIC. When LBIC data is taken at a series of voltages, one can in principle deduce the local J-V curves as well as local QE. Since an LBIC measurement gives the change in current between light and dark conditions, however, it must be corrected with dark J-V data to give the local illuminated J-V curve. This procedure assumes that either there is good light/dark superposition or that one can reliably correct for the lack of superposition. It also assumes that the dark J-V curve at

the local spot is not significantly different from the average dark curve. In practice, we have been able to make J-V comparisons, but not extract the full curves.

Figure 3-9 shows medium-resolution 638-nm QE maps at three biases for two different CIGS cells. The top row is from a cell with well-behaved J-V characteristics. There are four defects that do not change with bias, and in fact the map changes very little. The average QE is slightly reduced in forward bias, about 1% at 200 mV, and the response is slightly less uniform. In contrast, the bottom maps at the same biases are for a cell with distortion in its red J-V curve, much like the 23% Ga curve in Fig. 2-8. In this case, the average QE drops about 3%, and the forward-bias response is much less uniform, as one would expect from local variations in the amount of J-V distortion.

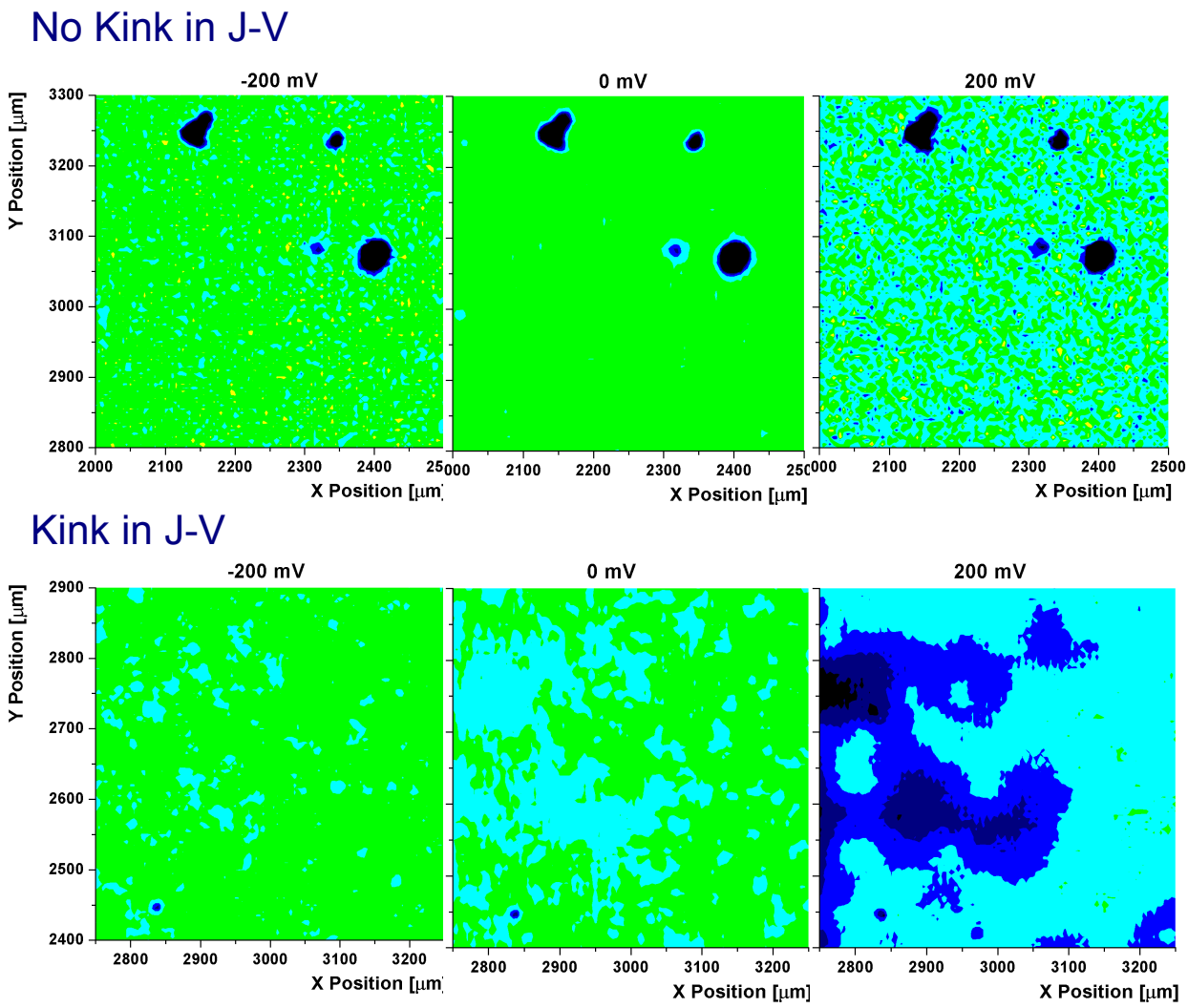

Figure 3-9. Red-light QE maps for CIGS cells with and without J-V distortion.

Figure 3-10 illustrates both the value of voltage-dependent LBIC and the difficulty in producing the full J-V curve. Two sets of data from low-resolution LBIC measurements at two small areas (about 10^{-6} of the total area) on a CIGS cell are shown. The curve with the more standard appearance is the J-V curve of the whole cell. The small-area curves track each other, which implies that there is simply better collection at the "A" point and that there is not a shunting or a diode difference. Since the total current for the small-area curves is about 10^{-6} that of the whole cell, reductions in fill factor and voltage are not unexpected, but the major distortion of the power-quadrant response and the forward-current limitation suggest that there is a major challenge in converting bias-dependent local QE measurements to a true J-V curve.

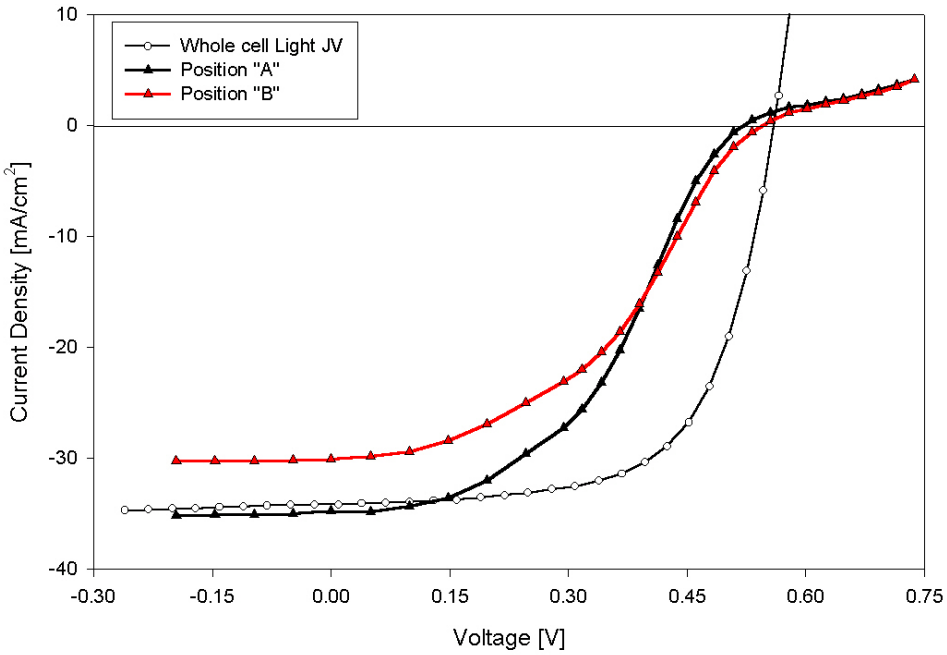

Figure 3-10. J-V from entire CIGS cell and two 10-µm local areas.

The LBIC work is being increasingly integrated with loss analysis and stress-induced changes in collaboration with David Albin's program at NREL. Much of the small-spot work from Section 3, as well as a description of the LBIC technique generally, will be presented in an invited talk by Prof. Sites at the 31st Photovoltaics Specialists Conference in January 2005.

4. DEFECT STUDIES

4.1. Defects in Evaporated and Selenized CIGS(S). Pam Johnson, in collaboration with David Cohen and Jennifer Heath at Oregon and Kannan Ramanathan at NREL, compared the defect densities of evaporated and selenized CIGS(S) cells. Current-voltage, admittance spectroscopy, and drive-level capacitance profiling measurements were taken on devices which were made with the two types of absorbers. One set of absorbers was deposited with physical vapor deposition at NREL [14], while the other set was made by selenization of metal precursors in an industrial environment at Siemens (now Shell) Solar Industries [15]. Several cells of each type were completed at NREL with one of two buffer treatments: a CdS layer or a cadmium partial electrolyte (Cd-PE) surface modification [16].

Illuminated J-V curves from each of the four cell combinations are shown in Fig. 4-1. The evaporated cells had higher voltages than the selenized ones, even after adjustment for band-gap differences, and the CdS buffers yielded higher voltages than Cd-PE. Furthermore, admittance spectroscopy (AS) data (Fig. 4-2) showed that the evaporated cells had little capacitance variation with frequency, while the selenized cells had a much larger variation between high and low frequencies.

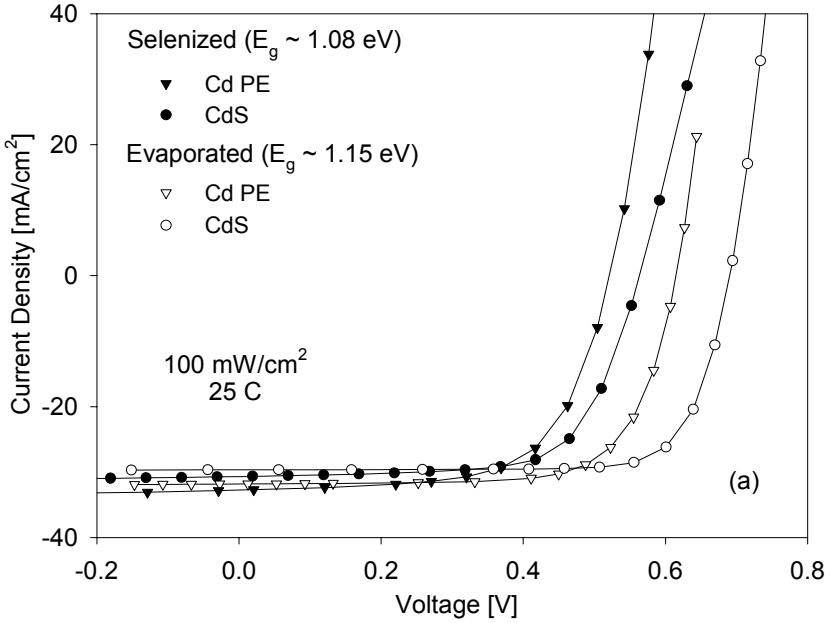

Figure 4-1. J-V curves for the four types of CIGS(S)S cells.

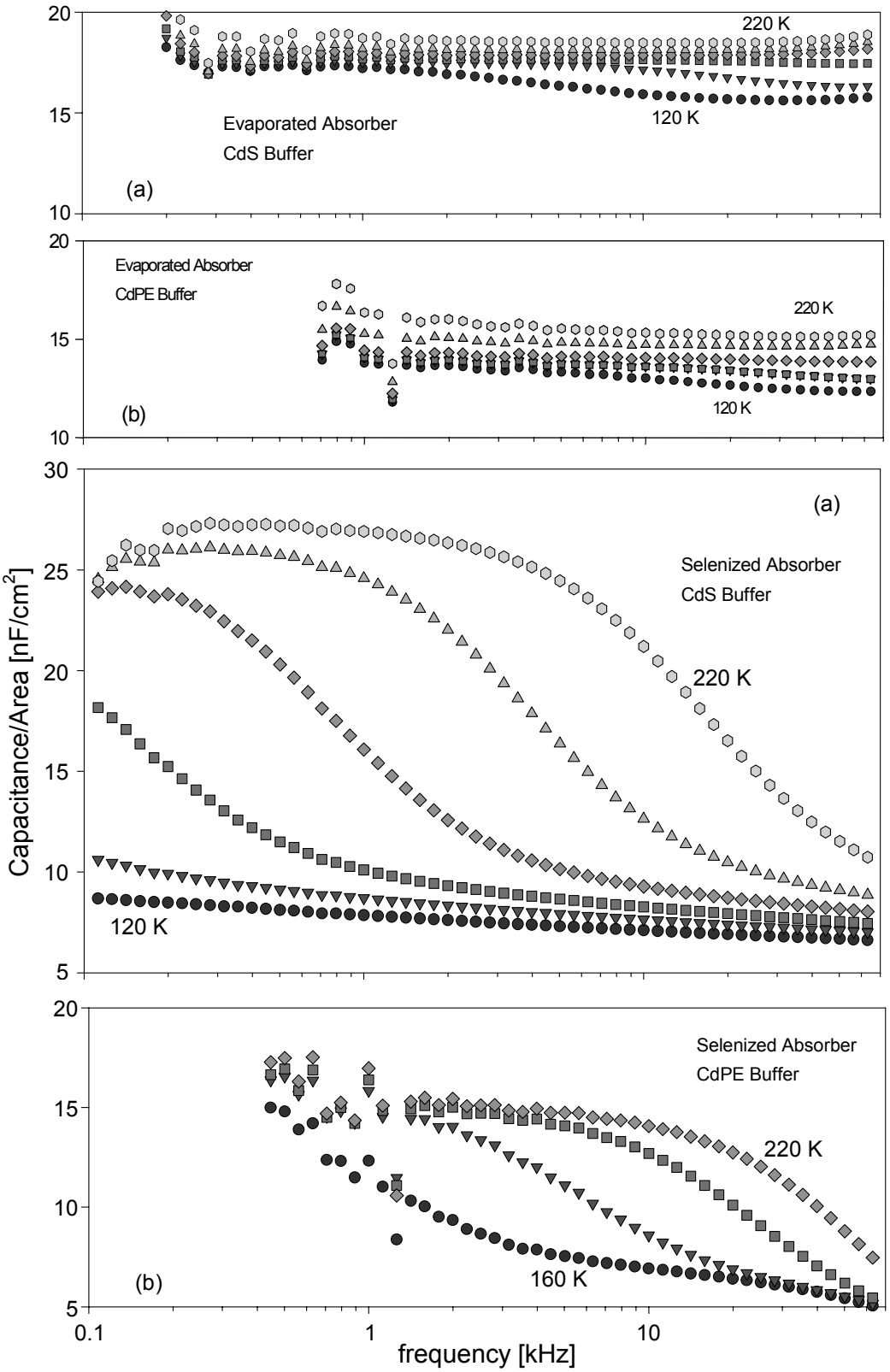

Figure 4-2. AS results for the four types of CIGS(S) cells.

A downward step in a capacitance-versus-frequency isotherm is indicative of a transition from a frequency-temperature region where a defect responds (i.e. where it traps and releases carriers at a rate greater than the measurement frequency) to a region where the same defect is not able to respond to the applied frequency. The broader transitions seen in this work indicate a range of defect energies.

Defect levels can affect the solar cells in at least two ways: shallower levels may improve device performance by contributing carriers at room temperature, while deeper levels can detract from device performance by enhancing recombination. We assumed a simple model in which the high-frequency capacitance reflects the response of the free-carrier density, while the low-frequency capacitance reflects the sum of the carrier plus trap densities. The evaporated devices in Figure 4-2 showed only small changes in capacitance with frequency, indicative of a small density of defects acting as hole traps, while the selenized devices had significant frequency-dependence, indicative of a large density of hole traps.

Figure 4-2 also shows the high-frequency capacitance difference between the evaporated and selenized cells. Assuming that there is no significant charge density at the interface, and the absorbers are reasonably uniform spatially, the evaporated devices indicate a free carrier (hole) density in the low-10^{15} cm^{-3} range, while the selenized devices had high-frequency values that indicate an approximate free carrier (hole) density in the mid-10^{14} cm^{-3} range. Thus, AS suggests that there are more free carriers, as well as fewer trapping defects, in the evaporated devices. The approximate free-carrier and trapping densities are summarized in the table with Fig 4-3.

The drive-level-capacitance-profiling (DLCP) technique [17] was employed to profile the defect density as a function of distance from the materials interface of the CIGS(S) and the adjoining buffer/window layer. Typical DLCP data at 11 kHz for both types of selenized cell are displayed in Figure 4-3. They clearly show the limiting high and low temperature responses and can hence be used to estimate the free carrier density p and the density of trapping-state defects N_t. The sum of N_t and p, labeled $N_{DL\ max}$ in Figure 4-3, is the high-temperature limiting value of the measurement. The DLCP results are included in the Fig. 4-3 table for comparison with AS.

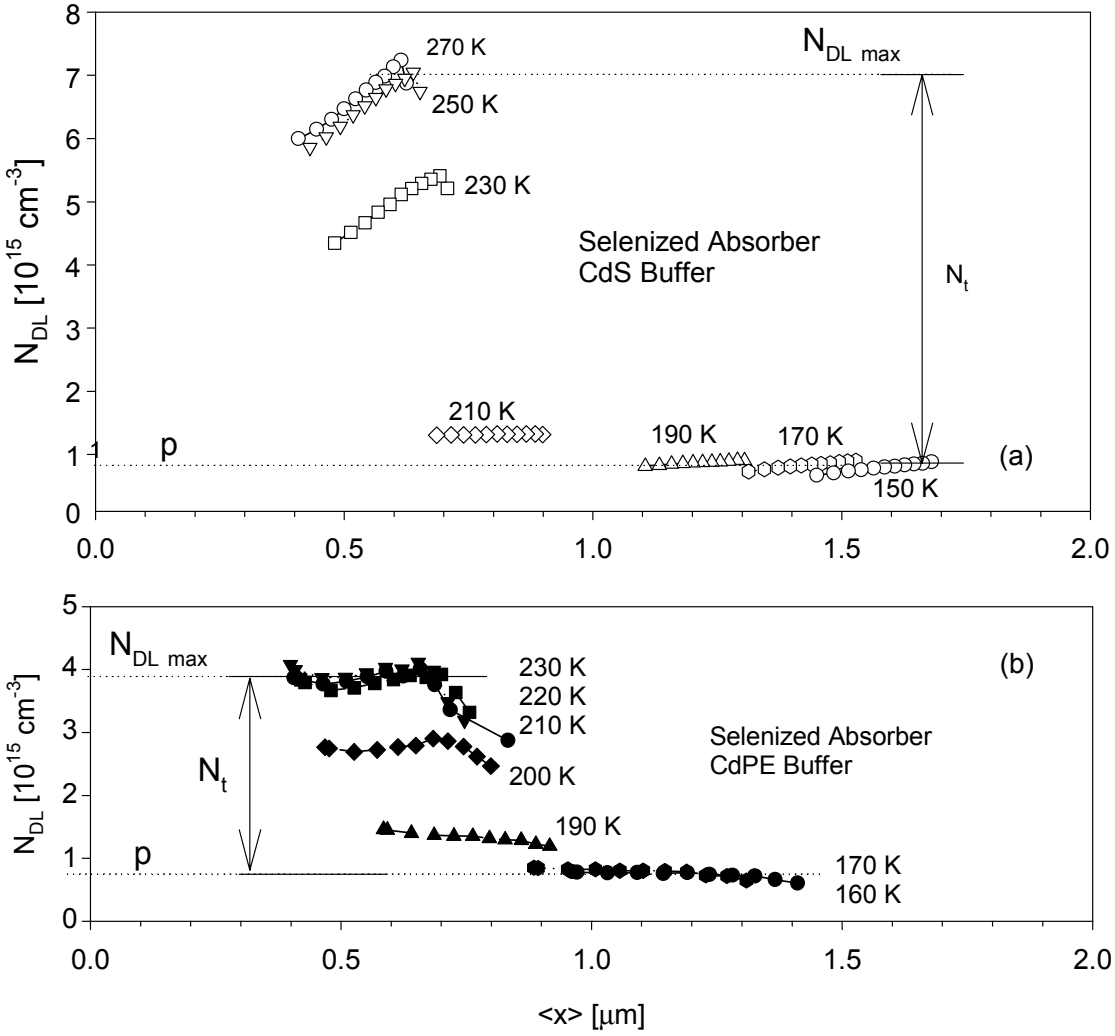

Device	Estimated Free Carrier Density from AS (cm^{-3})	Estimated Free Carrier Density from DLCP (cm^{-3})	Estimated Trapping State Density from AS (cm^{-3})	Estimated Trapping State Density from DLCP (cm^{-3})
Evaporated CdS	low 10^{15}	Not accessible	mid 10^{14}	Not accessible
Evaporated Cd	low 10^{15}	Not accessible	mid 10^{14}	Not accessible
Selenized CdS	mid 10^{14}	mid-high 10^{14}	mid 10^{15}	6 x 10^{15}
Selenized Cd PE	mid 10^{14}	mid-high 10^{14}	low 10^{15}	3 x 10^{15}

Figure 4-3. DLCP results from cells with CdS and Cd-PE buffers on selenized absorbers. Table summarizes AS and DLCP results.

The DLCP results for the two selenized devices exhibit a significant difference in defect response as a function of temperature. The measurement frequency of 11 kHz was

chosen, because it is high enough to provide good signal-to noise, and it also allows observation of the full defect response above 250 K, but only the free-carrier response below 160 K. Thus, at this frequency, the convenient 150-300 K temperature range allowed DLCP to span the full range of possible defect responses. From the data plotted in Fig. 4-3, we deduce a free carrier density in the mid-10^{14} cm^{-3} range for both types of selenized devices, a trap density of approximately 6 x 10^{15} cm^{-3} for the selenized CdS device, and a slightly lower trap density for the selenized Cd PE device. These DLCP trends and values are consistent with the results from AS. The relatively low voltage of the selenized cells is likely the result of the higher defect density and lower carrier density.

The evaporated samples were not conducive to DLCP analysis, because their response showed a steep spatial variation in state density and little variation with temperature. The lack of significant variation of defect response with temperature is consistent with the minimal defect response of AS measurements taken in the same temperature range. The minimal temperature variation of the DLCP data, together with the small step in the AS data, indicate that the density of trapping defects affecting these devices is quite low. In fact, the average estimated trap density of these two devices from the AS data was 5 x 10^{14} cm^{-3}, nearly an order of magnitude below the selenized devices.

The comparative study of CIGS(S) showed significantly larger defect densities in selenized than in evaporated absorbers. Additionally, the activation energy derived from the temperature dependence in Fig. 4-2 was consistently larger for the selenized cells. The defect differences between the CdS and the Cd-PE buffers were relatively modest, but those with the CdS buffers were somewhat larger. The conclusion is that the selenized cells had deeper states and smaller carrier density, while the evaporated cells have shallower states and thus a higher carrier density. These results strongly suggest that the larger values of V_{OC} in the evaporated-absorber solar cells are a result of not only the larger estimated free-carrier densities, but also of the smaller trapping-state densities. A paper, "Comparative Study of Defect States in Evaporated and Selenized CIGS(S) Solar Cells," has been submitted for publication in Progress in Photovoltaics.

4.2. Photoluminescence of Poly- and Single-Crystalline CdTe. Caroline Corwine, in collaboration with Tim Gessert, Pat Dippo, Wyatt Metzger, and Anna Duda at NREL, has made systematic photoluminescence (PL) measurements on poly- and single-crystalline CdTe. The objective has been to explore what combinations of single-crystal Cu diffusion and/or annealing in various gasses were necessary to replicate the PL response from the polycrystalline thin-film CdTe that is used in solar cells.

The single-crystal samples used in this study (1 cm x 1 cm x 0.1 cm) were cut from 99.9999%-purity wafers from one crystal grown by the vertical Bridgman technique. The wafers were mechanically polished by the manufacturer (Keystone Crystals), and except for rinsing with acetone and methanol, no other chemical surface treatments were performed before or after metallization and/or annealing. The polycrystalline thin-film CdTe samples used for comparison purposes were produced by NREL (close-space sublimation) and First Solar, LLC (vapor-transport deposition). The structure of the thin-film samples was glass/SnO_2:F/CdS/CdTe.

Photoluminescence (PL) was taken on all samples shortly at 4.5 K in a helium closed-cycle cryostat. In most cases, a HeNe laser (λ = 632.8 nm, or E_g = 1.960 eV) was used for excitation, and a long-pass filter (695 nm) was used to suppress reflected HeNe laser light. PL spectra were collected by a grating spectrometer, and all spectra were corrected for the spectrometer response. The PL spectra were analyzed by fitting the measured spectra to series of Gaussian curves. This process enhanced the separation between primary transitions and their 21-meV phonon replicas, and resulted in a measurement uncertainty of about 1 meV.

Figure 4-4 shows PL spectra from an untreated crystalline control samples and from samples annealed at 400°C for 1 hr in O_2, N_2, and forming gas (10% H_2/90% N_2), all with no copper added. The O_2- and N_2-annealed spectra showed little change. Further, the excitonic PL peak positions of the sample annealed in O_2 were consistent with other reports [18]. In contrast, annealing in forming gas eliminated the 1.587 eV peak seen in both the non-annealed and the O_2- and N_2- annealed samples, and more clearly delineates the 1.591 eV shoulder. This result is significant, since forming gas would be expected to reduce residual surface oxide.

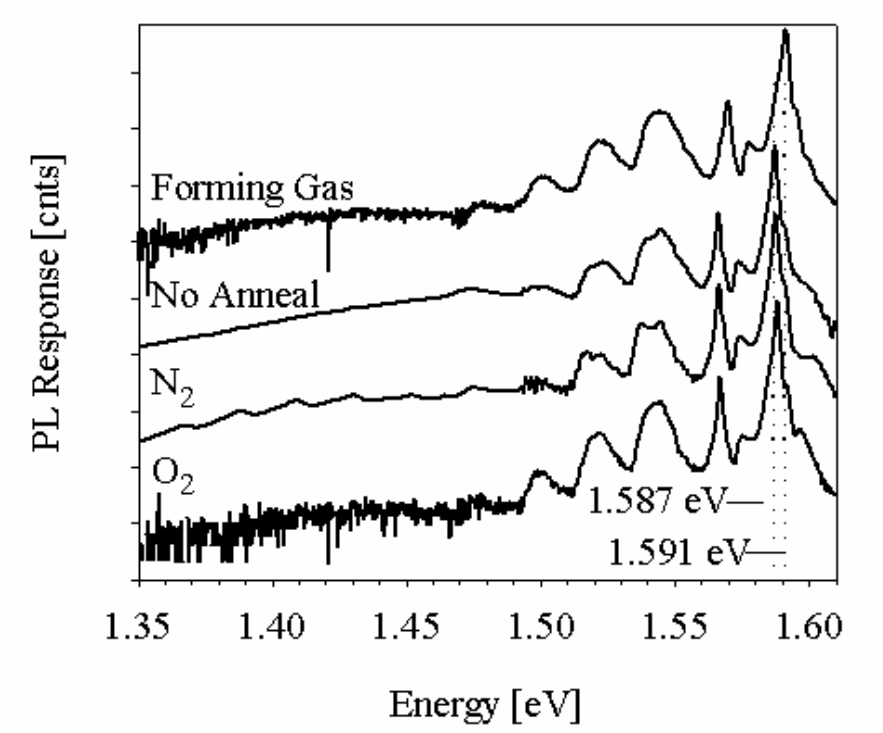

Figure 4-4. PL from CdTe single crystals with four anneal conditions and no intentional Cu. Spectra offset by factors of 10 for clarity.

For a second series of measurements, 10-nm layers of 99.999%-pure Cu were deposited onto single-crystal CdTe using electron-beam evaporation. Figure 4-5a shows PL from the Cu-diffused samples following annealing in forming gas, N_2, 20% O_2 + 80% N_2 (air-like), and O_2 ambients. In contrast to Fig. 4-4, all spectra in Fig. 4-5a reveal significant changes in the high-energy peaks, and the elimination of the peaks related to a zero phonon line at 1.54 eV.

Figure 4-5a also shows that diffusion of Cu into CdTe under a N_2 ambient (a typical process for Cu-contact diffusion in CdS/CdTe solar cells [19]) produces the smooth broad peak centered at ~1.45 eV. An otherwise identical sample annealed in forming gas had a similar broad spectra and also new higher energy peaks, each with several distinct phonon replicas. However, the ambient that produced the most striking effect was O_2. Here the broad peak is again observed, but now a clear zero-phonon peak is seen at 1.456 eV with several phonon replicas. This peak does not appear in any of the non-Cu samples, nor in the Cu sample annealed in N_2 or forming gas. It is, however, observed to

a lesser extent in the Cu sample annealed in the air-like ambient (i.e., 20% O_2 + 80% N_2). The absence of the 1.456 eV peak in reducing or non-oxidizing ambients, coupled with its increasing presence in progressively oxidizing ambients, strongly suggests that it is the signature of a defect related to both copper and oxygen.

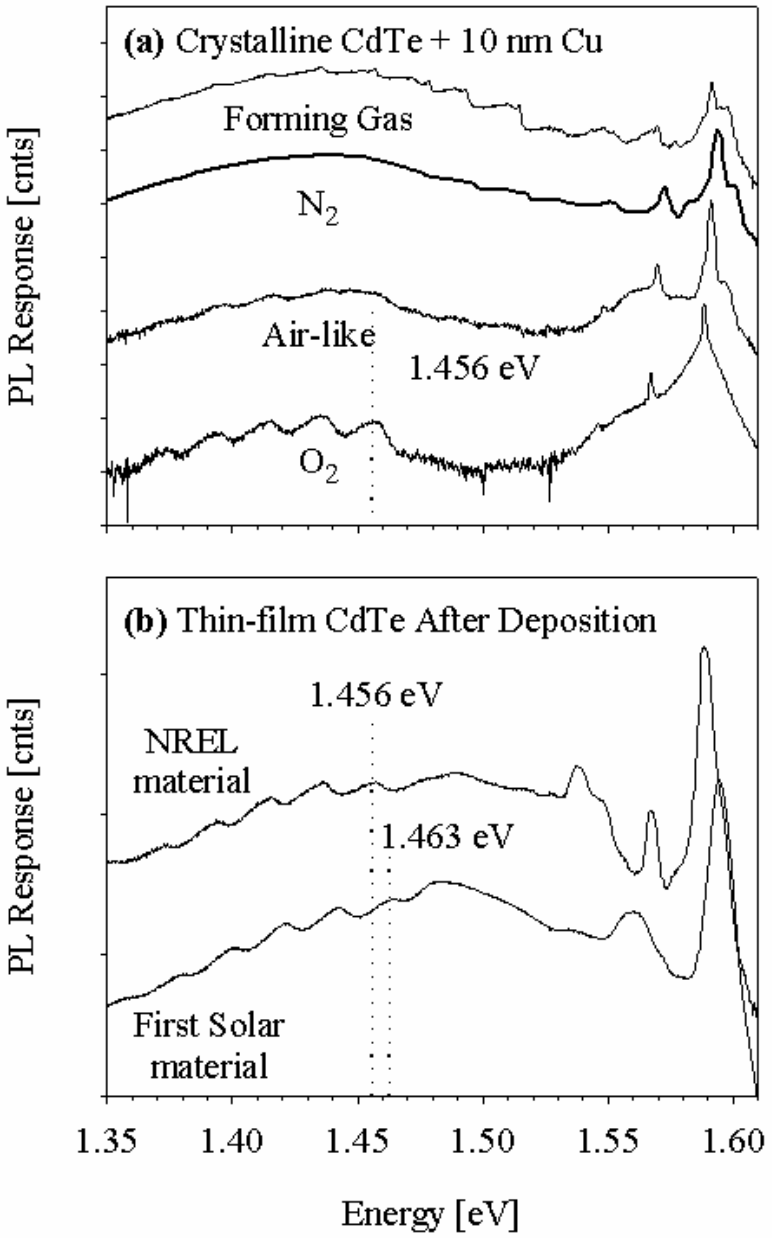

Figure 4-5. (a) PL spectra of single-crystal CdTe coated with 10 nm Cu and annealed with four ambient gasses. (b) PL spectra for as-deposited polycrystalline CdTe films from two laboratories. Spectra offset by factors of 10 for clarity.

Figure 4-5b shows low-temperature PL spectra from two as-deposited CdTe polycrystalline films. The film produced at NREL reveals the same 1.456 eV zero-phonon line observed in the single-crystal Cu samples annealed in the oxidizing atmosphere, and an additional peak at 1.489 eV. The PL spectra of the film from First Solar is similar, revealing zero-phonon lines at 1.463 eV and 1.481 eV. It is noted that neither the 1.489 eV nor 1.481 eV peaks would produce phonon replicas at 1.456 eV or 1.463 eV. Further, annealing of the First Solar films in N_2 at 400°C (not shown) retains the 1.463 eV peak but eliminates the 1.481 eV peak, indicating that the two peaks have different origins. The 7 meV difference between the 1.463 eV peak and the one at 1.456 eV seen in the NREL film and crystalline samples suggests that growth conditions may influence the position of this defect. Nevertheless, the observation of what is presumed to be a common peak in both the thin-film and oxygen-annealed crystalline samples containing copper suggests that a defect related to a combination of copper and oxygen is present in the films.

Since the 1.456 peak appears only when both Cu and O_2 are involved, it follows that the polycrystalline CdTe used in solar cells contains a dominant defect complex involving both Cu and O. Oxygen tends to form an isovalent defect in CdTe, namely O_{Te}, which is electronegative. In contrast, Cu is amphoteric (i.e., a Cu_i donor will form as readily as a Cu_{Cd} acceptor). Because the Cu_i defect is electropositive, and O is more electronegative than Te, it is likely that these two defects form a donor complex Cu_i-O_{Te}, and the resulting activation energy is 100–150 meV [20]. This activation energy is consistent with intensity-dependent PL measurements that suggest that the 1.456 eV peak is a band-to-defect transition. A paper on this work, "CdTe photoluminescsnce: Comparison of solar-cell material with surface-modified crystals," is in preparation for submission to Applied Physics Letters.

5. NUMERICAL SIMULATION

5.1. Simulation Tools and Baselines. We have given a high priority to improve the foundation for numerical simulation of thin-film polycrystalline solar cells. This process included a survey of available software by Alan Fahrenbruch, which is summarized below. The packages followed by (**) are have been in use by Colorado State.

SOLAR-CELL-SPECIFIC SOFTWARE:

AMPS**	S. Fonash	free by request
ADEPT**	J. Gray	free by request
PC1D	P. Basore	≈ $100
SCAPS**	M.Burgelman	free by request
SimWindows**	D. Winston	free by download

SEMICONDUCTOR-DEVICE SOFTWARE:

	PLATFORM	DEMO	ACADEMIC	PROF.
APSYS	Windows, ???	Free	$16,500	$33k
Atlas	UNIX, Windows	—	$2,900	$60k
DESSIS**	UNIX, Windows	—	$1,900	$50k–$150k
Medici	Solaris, Unix, LINUX	?	?	?
MicroTec	Windows	Free	$700	?

CIRCUIT-MODELING SOFTWARE:

Pspice** Student version by download; professional version about $2000. Can be used to add external series resistance or analyze module circuits.

The solar-cell-specific packages listed are all 1-D, they all use a drift/diffusion transport model, they all run efficiently on newer windows machines, and they yield very nearly the same results. The semiconductor device packages are more versatile, but are pricier and more challenging to use. We have been very pleased with the DESSIS software that we have been able to use at NREL for 2-D grain-boundary simulations. We have also found the student version of Pspice very useful for simple circuit simulations, and the professional version for more involved circuits.

For consistent comparison of numerical simulations between laboratories and software packages, we adopted a set of baseline parameters for both CIGS and CdTe cells, which are listed in M. Gloeckler, A.L Fahrenbruch, and J.R. Sites, "Numerical modeling of CIGS and CdTe Solar Cells: Setting the Baseline," Proc. 3rd World Conf. on Photovoltaic

Energy Conversion, 491-494 (2003). For both CIGS and CdTe, we deliberately used a minimal cell configuration of three layers (TCO/window/absorber). The parameters chosen were our best estimates for "typical" high-efficiency cells at room temperature. We and others have modified this baseline to study specific cell features, but we have found considerable merit in defining a common starting point. The J-V that follow from our base-line parameters, and QE curves with minor modification are shown in Fig. 5-1. The key changes necessary to reproduce specific experimental results are the densities of deep and shallow acceptor levels in the buffers and absorbers, the capture cross sections, and in the case of CIGS, the band offset with CdS.

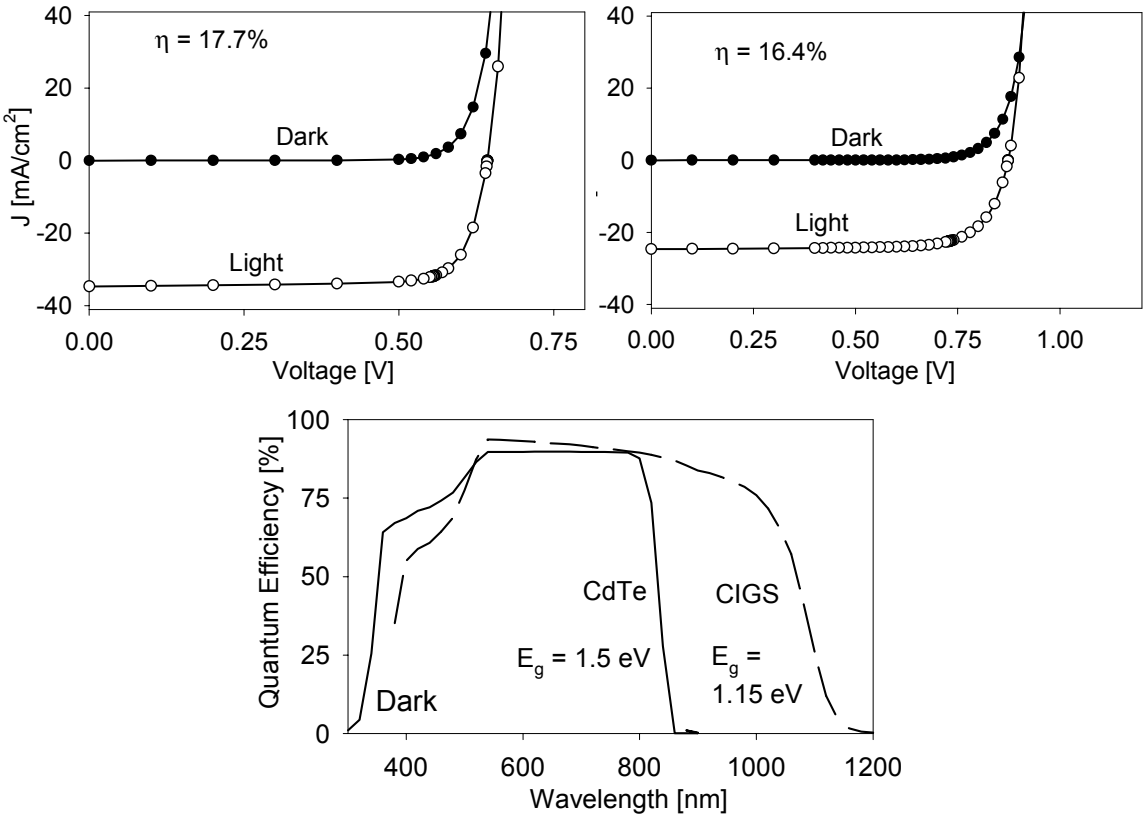

Figure 5-1. Simulation baseline J-V curves for CIGS (top left) and CdTe (top right) and for QE of both cell types (bottom).

5.2. CdTe Simulations. A major simulation project with CdS/CdTe cells, now largely completed by Markus Gloeckler [J. Appl. Phys. **95**, 4438-4445 (2004) and Proc. EPVSEC-19 (2004)], has been the explanation of several effects observed in quantum-efficiency measurements made in forward bias and under non-standard light conditions.

Various effects may be due to the voltage dependence of collection efficiency, the series resistance of the cell and instrumentation, an electrical barrier at the back contact, photoconductance of the CdS or CdTe, a secondary barrier in the primary junction, or a combination of these. Historically, there has been a problem with the interpretation of QE from both CdTe and CI(G)S cells, because without consideration of all possibilities, an experimental QE feature may be assigned to the wrong physical mechanism. Hence, we have advocated that measured QE be referred to as "apparent quantum efficiency" (AQE), at least until interpretation issues are resolved.

The simulations shown in Figure 5-2 are based on our three-layer baseline model for CdTe with the addition of a back-contact barrier. The results very nearly replicate the experimental work of Bätzner et al [21] if one interprets ac phase angles above 90° as an AQE sign reversal. Clearly there are several different features illustrated in Fig. 5-2. The "standard" decrease in AQE at the intermediate wavelengths is due to resistance in the cell and the measurement equipment [22,23]. The fact that this QE becomes slightly negative at high biases is a result of modest light-induced changes in series resistance and A-factor.

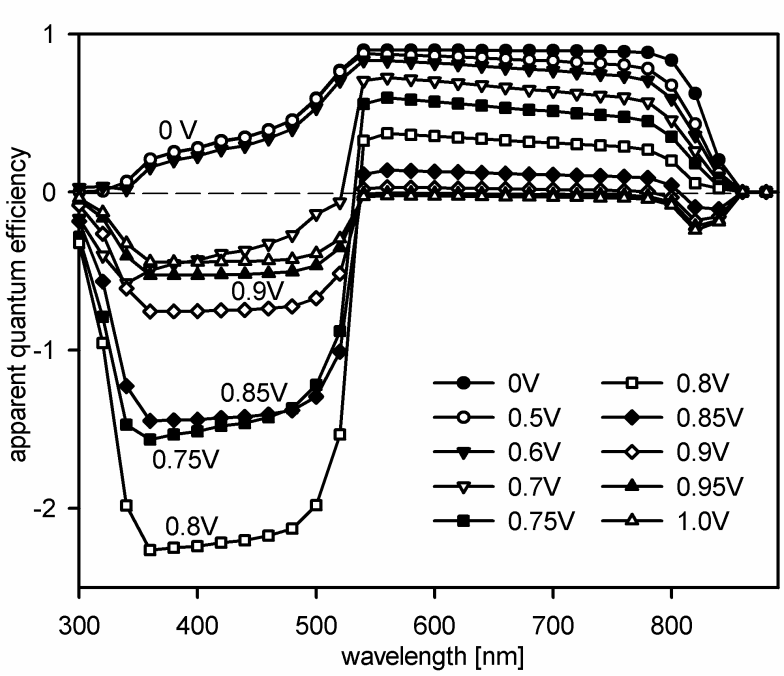

Figure 5-2. Calculated voltage dependence of CdTe AQE.

The large negative peak below 500 nm in Fig. 5-2 is basically a phototransistor effect where blue photons pull down the CdS conduction band and allow considerably more forward current (opposite sign from photocurrent) to flow. This peak is highly sensitive to the intensity of the probe beam used to measure AQE. Since AQE is determined by normalizing the current change to photon flux, it will be quite large when the probe intensity is small. At higher probe intensities, the CdS-related AQE effect becomes quite small. Since the experimental photon flux generally varies with wavelength in a QE measurement, both the size and the shape of the CdS-related peak will be highly instrument and calibration dependent even for measurements made on the same or similar cells.

The numerical model of Fig. 5-2 also reproduces the small negative band-gap peak that is reported in Ref. [21]. This negative response is caused by deep absorption of photons that have energies near the band gap energy of CdTe and are thus absorbed in the secondary space charge region resulting from the contact barrier at the back of the device. The back diode is in reverse bias when the complete device is under forward bias, and hence the back diode has an increased space charge region at higher voltage. Electron-hole pairs generated towards the back contact intrinsically generate a current response opposite to the primary photocurrent. This effect would not be present in the absence of a back-contact barrier.

The back-contact barrier can also affect the analysis of light and dark J-V curves. Fig 5-3 shows simulated J-V curves for a small back-contact barrier (0.3 eV) and a more significant one (0.5 eV). In each case, there is also a comparison between smaller (7 x 10^{13} cm^{-2}) and larger (6 x 10^{14} cm^{-2}) carrier densities. The small-barrier, larger-density curves (triangles) represent today's best CdTe cells and show little sign of rollover at higher voltage. The small-barrier, smaller-carrier-density curves (circles) show a slightly smaller voltage, but are otherwise very similar. With the large contact barrier and large density (inverted triangles), there is reduced fill-factor and significant rollover in the light and a nearly flat curve in the dark. If one also reduces the carrier density (squares), the open-circuit voltage is significantly reduced. The transition from the low-barrier cases to the high-barrier ones is very suggestive of effects seen after elevated-temperature stress.

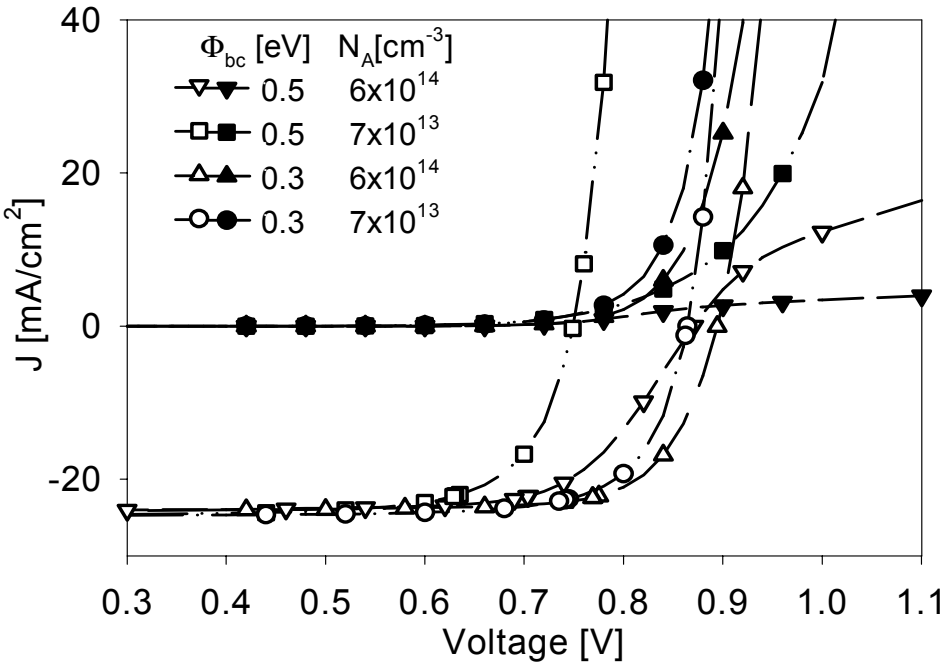

Figure 5-3. Simulated light (open symbols) and dark (filled) J-V characteristics for CdTe cells. Large and small back-contact barriers, plus larger and smaller carrier densities compared. CdTe thickness 4 μm.

Implicit in the Fig. 5-3 curves is that crossover of light and dark curves is a general consequence of a large back-contact barrier. In fact, the crossover is present to smaller degree with the small-barrier curves, where it occurs at currents off the scale shown. Such crossover, especially when it is relatively subtle, can be misinterpreted as a large decrease in photovoltaic collection efficiency in the vicinity of the open-circuit voltage. This situation is illustrated in Fig. 5-4, which plots the apparent collection efficiency for different barrier heights. The curve labeled "depletion-width approximation" is the calculated collection efficiency in the absence of a back-contact barrier, series resistance or other complications. It is very flat throughout the operating region of the cell, but falls towards zero at the flat-band voltage, which is significantly above V_{OC}. With a back-contact barrier, even an otherwise modest one, the apparent collection efficiency falls to zero at the crossover voltage. At the same time, V_{OC} decreases, but only a small amount (compare triangles and inverted triangles in Fig. 5-3). The problem is that crossover due to the back contact may be misinterpreted as a major reduction in collection efficiency

even at voltages below V_{OC}. The same problem can occur for crossover due to series resistance or any other effect.

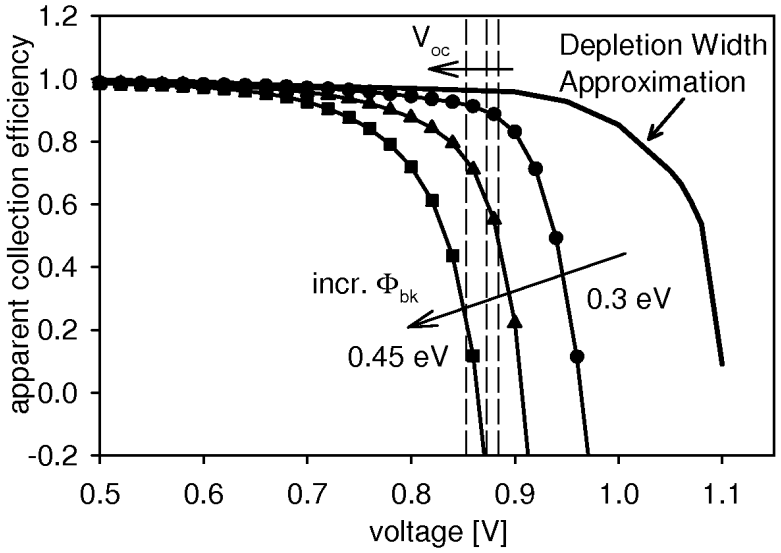

Figure 5-4. Apparent decrease in CdTe collection efficiency due to the back-contact barrier Φ_{bk}.

Two other CdTe simulation projects are illustrated below. In one (Fig. 5-5), Alan Fahrenbruch showed the capacitance simulation capability of the SCAPS software. He converted experimental and simulated capacitance vs. voltage curves to hole density vs. distance from the CdS junction, and he was able to make very respectable fits (squares) to the experimental data (circles) under both light and dark conditions. The results show the amount of carrier-density increase due to photogeneration and the shift of the spatial region probed towards the CdS junction. In the other project, Jun Pan simulated QE as a function of CdTe thickness and compared those results with experiments done at the University of Toledo. Figure 5-6 shows the experimental QE normalized to Toledo's J_{SC} values and the corresponding QE simulations for the same thicknesses. The simulations for thinner absorbers are sensitive to the back surface reflection chosen, which in this case was chosen to be 50%. There is a general similarity between experiment and simulation, but two clear differences. The simulation does not reproduce the red falloff for thick-absorber cells, likely because experimental TCO absorption increases towards the red. More importantly, the experimental QE for thinner cells shows a small decrease even at short wavelengths, which currently does not have a satisfactory explanation.

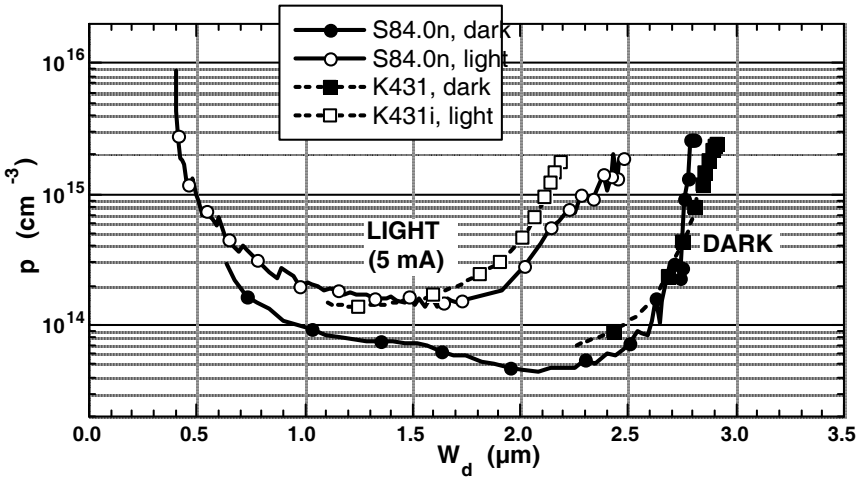

Figure 5-5. Experiment (squares)/simulation (circles) carrier-density comparison.

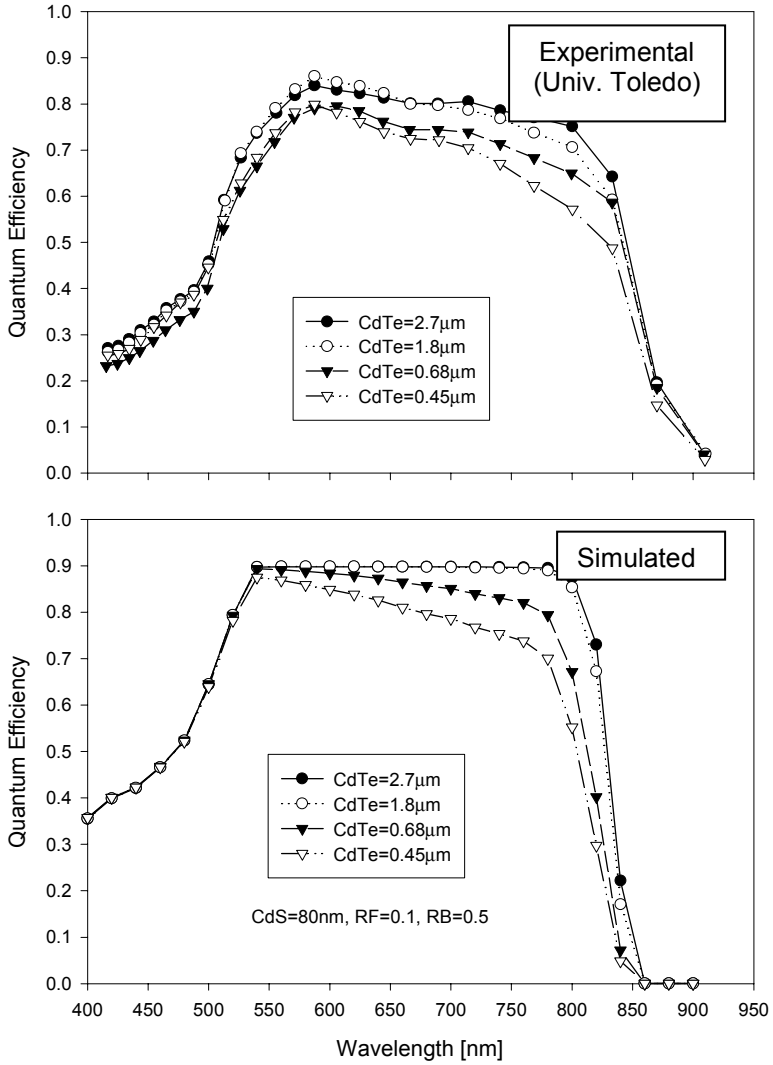

Figure 5-6. Experimental and simulated QE variations with CdTe thickness.

5.3. CIGS Simulations. Much of the CIGS simulation work has focused on the effects on the conduction-band offset between CdS and CIGS. The band picture for CdS/CIGS, including the offset, was shown in Section 2 (Fig. 2-6) for different Ga concentrations. The low-Ga, or large spike, part of the figure is responsible for the non-superposition and red-kink results described in Section 2. Equally important, however, is the larger-Ga regime, where the offset changes to a cliff, and experimentally the voltage of such cells has been limited. Simulations of this wide-gap region have been performed by Markus Gloeckler, and a manuscript, "Efficiency Limitations for Wide-Band-Gap Chalcopyrite Cells," has been accepted for publication in Thin Solid Films.

Although a spike offset can impede photovoltaic collection, it also renders states near the CdS interface ineffective for forward-current recombination. In fact, the highest efficiency CIGS cells with E_g near 1.15 eV have very nearly the optimal magnitude of the spike, about 0.3 eV. Higher-gap cells with the cliff offset, however, do not effectively shield the photoelectrons from the interfacial states that can degrade photovoltaic performance. Our simulation results of voltage and efficiency for the full range of conduction-band offsets, or alternatively CIGS band gap on the top scale, are presented in Fig. 5-7. Several different degrees of interfacial recombination are shown using interfacial recombination velocity v_{intf} as a fraction of thermal velocity v_{th} ($\sim 10^7$ cm/s) is used as the recombination parameter. The low-gap portion of Fig. 5-7, where the spike is predicted to limit current, is also noted. Current and fill-factor were calculated for all conditions, but they are less affected by the amount of interfacial recombination.

In the absence of interfacial recombination ($v_{intf} = 0$), V_{OC} should increase linearly with band gap. Even small amounts of interfacial recombination, however, will limit the voltage in the small-spike or cliff regions ($\Delta E_C \leq 0.1$ eV, or $E_g \geq 1.3$ eV), and the simulations predict that voltage will become band-gap independent at higher gaps. These results are consistent with experimental measurements of voltage vs. band gap [24,25] and with analytical predictions [26] and simulations of varying offset at constant band gap [27]. There may of course be other reasons why the voltage and efficiency of high-gap CIGS cells are limited, but even if that is so, interfacial recombination is likely to further reduce the high-gap efficiency.

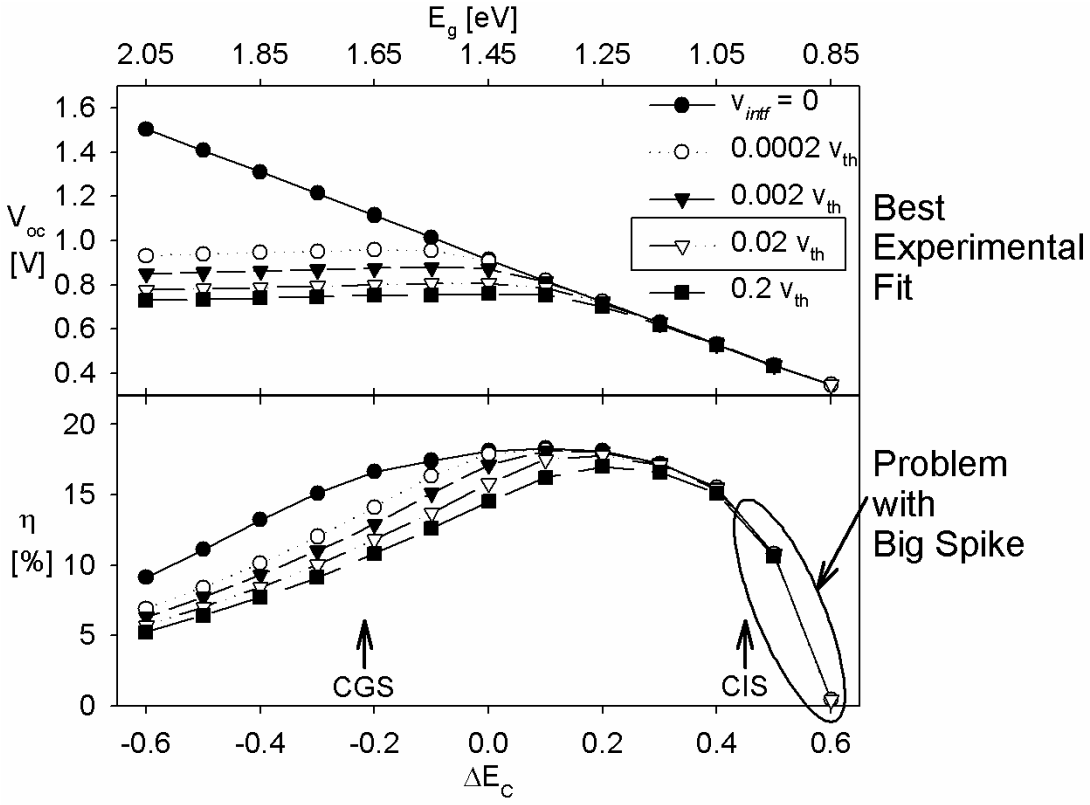

Figure 5-7. Simulated effect of interfacial recombination on CIGS voltage and efficiency as a function of band offset.

Also shown in Fig. 5-7 is what would happen if the conduction-band offset were too large (big-spike region). Near $\Delta E_C = 0.45$ eV, photocurrent starts to become blocked, and by 0.6 eV, the photocurrent, and hence the efficiency, have dropped to zero.

A possible solution to the interfacial-recombination problem is to use an alternative window layer with high-gap CIGS so that the combination yields the preferred small-spike conduction-band offset. Figure 5-8, where the window/absorber band alignment is set to +0.9, +0.6, +0.3, and 0 eV, respectively, for a 1.15 eV absorber material, illustrates the possibilities. The +0.3 curve, denoted BL for baseline, represents the CdS/CIGS cells from Fig. 5-7 with $v_{intf} = 0.2\ v_{th}$, and the other curves correspond to possible alternative window materials. When ΔE_C with respect to 1.15 eV is increased, the voltage where the band-gap-independent region begins is progressively larger, which could allow higher efficiency for the larger band-gaps. There is, however, a tradeoff in that the onset of photocurrent blockage will also occur at progressively larger band gaps.

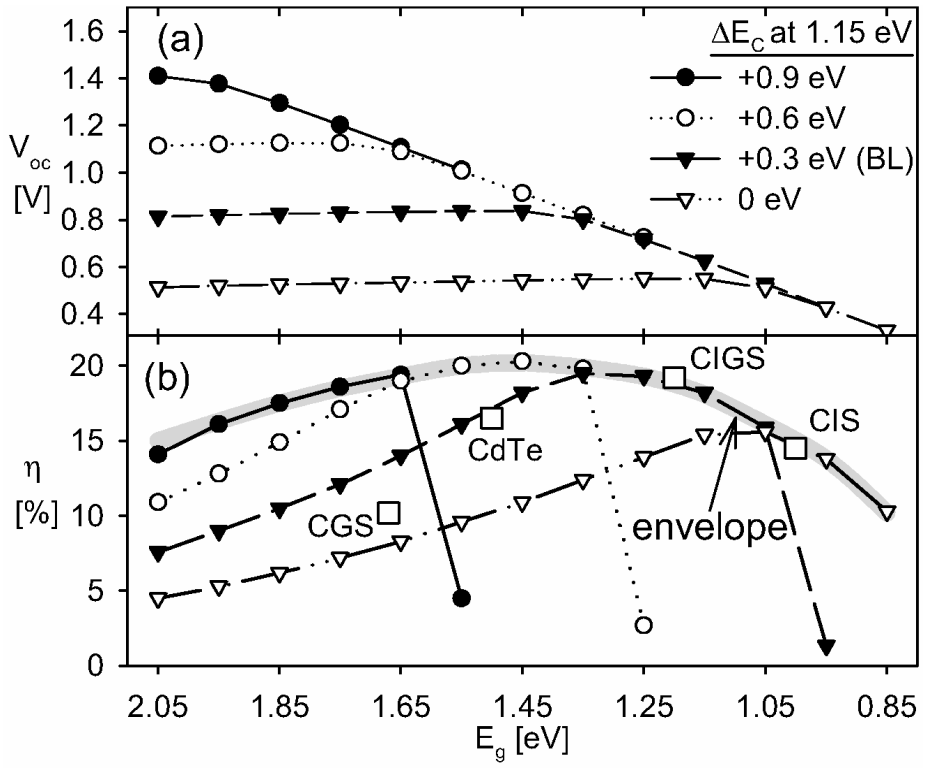

Figure 5-8. Calculated voltage and efficiency for different band alignments.

Note that the highest efficiencies to date for CdS/CIS, CdS/CIGS, and CdS/CdTe, which has a band alignment similar to CIGS of the same band gap, all fall along the inverted-triangle curve of Fig. 5-8. CdS/CGS, however, falls below this curve, which implies that band alignment is not the only mechanism that is currently limiting its efficiency.

The envelope of the efficiency curves in Fig. 5-8 is the simulation result if one selects the optimal band alignment for each band gap, but holds the other simulation parameters constant. Each choice of window follows the envelope for approximately 0.3 eV, which implies that a single window material is unlikely to form good cells over a large range of CIGS band gaps. In particular, one will most likely want different windows for CIS and CGS cells.

Another CIGS simulation project that was completed recently was the impact of conduction-band grading on the performance of CdS/CIGS cells. This study was motivated by suggestions that if one engineered the spatial profile of the Ga/In ratio, and hence the CIGS band gap, it might be possible to optimize cell performance. Markus

Gloeckler considered three cases: a linear front grading, a linear back grading, and a combination of the two, referred to as a double grading. In each case, the minimum band gap, the front and/or back increase in gap (ΔE_{Fr} or ΔE_{Ba}), and the point d_{min} where the grading is terminated were systematically varied. In contrast to several reports in the literature, we were careful to separate the grading effect from performance changes due to varying a uniform band gap.

We found that back grading by itself can increase efficiency in standard-thickness cells by a small amount ($\leq$ 0.5%). Because it acts as a back reflector, however, it can have a more significant positive impact on cells made with thin ($\leq$ 1 μm) CIGS layers. Front grading alone is always detrimental and can have a negative effect on fill factor, which may reduce cell efficiency by several percent. The double-grading results are basically a combination of the two and are illustrated in Fig. 5-9.

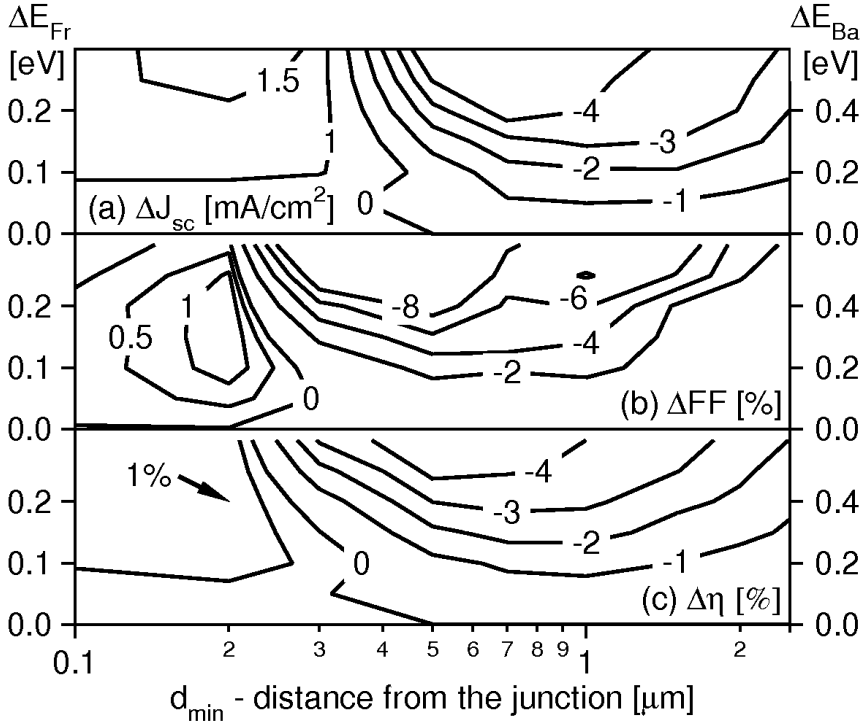

Figure 5-9. Changes in (a) current, (b) fill-factor, and (c) efficiency for double-graded CIGS cells when voltage is held constant.

In Figure 5-9, the data corresponds to a common effective band gap and hence a common voltage for comparison purposes. Current and fill-factor show modest improvements when the minimum in the graded band gap occurs midway through the

depletion region, but fairly significant reductions when the minimum is outside the depletion region. These reductions occur because the grading profile forms a barrier to current collection [28] that reduces current at all voltages, but becomes more severe with increasing voltage, and hence the fill-factor reduction as well. The grading results, consistent with recent experimental data [29], were presented at the 14th International Conference on Ternary and Multinary Compounds, and the manuscript, "Band-gap grading in Cu(In,Ga,)Se_2 solar cells," has been submitted for publication in the Journal of the Physics and Chemistry of Solids.

5.4. Two-Dimensional Grain-Boundary Simulations. A relatively new project has been the extension of simulation techniques to two dimensions for the primary purpose of examining grain boundaries (GBs) in polycrystalline cells. This project has been using the DESSIS software that NREL has made available. The part of DESSIS we are using is conceptually similar to AMPS and SCAPS with the capability of setting up a two-dimensional mesh. We are grateful to Wyatt Metzger for hosting Markus Gloeckler at NREL and orienting him to the DESSIS software capabilities.

To date, the GB simulation project has focused on CIGS cells, where the GBs appear to not harm solar-cell performance and perhaps actually improve it. There have been many suggestions as to why CIGS grain boundaries are benign or even helpful, but no general agreement so far. Our approach is to consider the different possibilities for how a grain boundary might affect cell performance and calculate the specific effects of each possibility. The possibilities we have considered include recombination centers at the grain boundary, a charge sheet at the grain boundary, and a band-gap expansion, seen primarily in the valence band, as one approaches the GB. Future work will consider combinations of these possibilities.

The set-up of a 2-D simulation is similar to a 1-D simulation in that one defines regions of the cell, assigns parameters to each, and establishes a mesh configuration. The mesh configuration needs closer attention in 2-D, because calculation time depends on the total number of mesh points. In practice, that means that it is important to have a fine mesh in regions where large changes are anticipated, but a coarse mesh otherwise.

The basic configuration for CIGS grain-boundary simulations is shown in Fig. 5-10. The basic three layers used for 1-D simulations (ZnO, CdS, and CIGS) are shown, as well as a vertical GB region where the CIGS parameters can be altered. Horizontal GBs have also been considered, and only have a significant effect if they are in the depletion region or block the flow of current. The GB region shown in Fig. 5-10 has been assigned recombination states denoted by a "surface" recombination velocity S_{GB}, a charge sheet, which can be positive or negative, or a variation in the valence band ΔE_V. The width of the GB region can be varied, but in general, the GB effects are not very sensitive to this width.

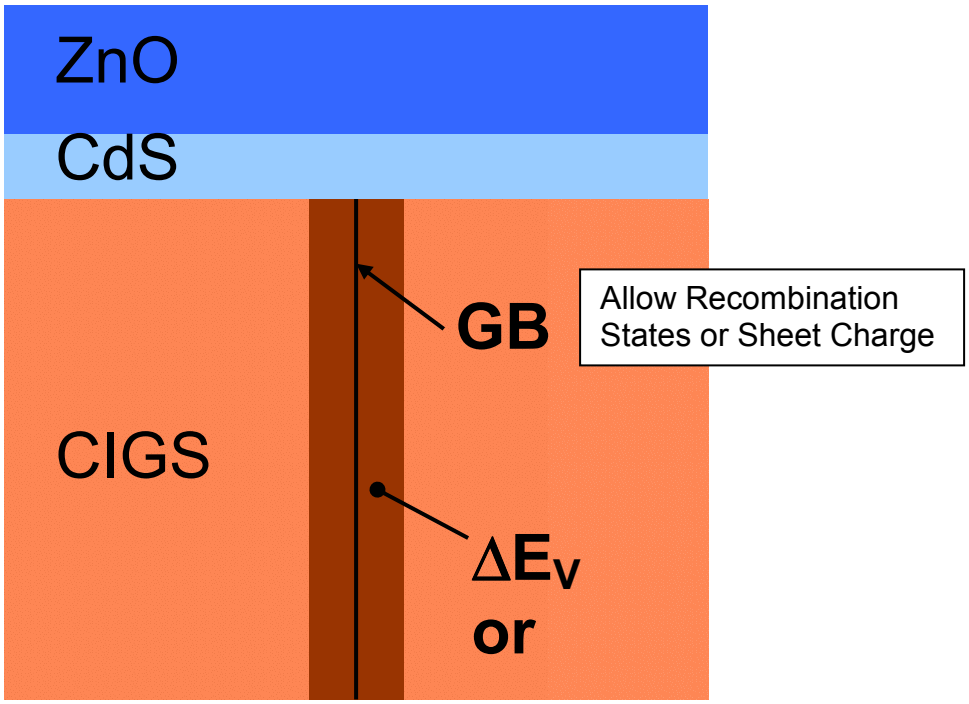

Figure 5-10. Basic configuration used for CIGS grain-boundary simulations.

Placing recombination states at the GB reduces the performance of the solar cell by an amount that increases with increasing S_{GB}. Unless the grains are very wide, however, GB recombination states are indistinguishable from additional bulk recombination states. If the recombination states are only placed on part of the GB, we find, as one might expect, that those in the depletion region will reduce voltage whereas those past the depletion region will limit current.

Investigation of the effect of charge at the GB yielded results that may be somewhat surprising. A positive charge at the GB will produce dips in both the conduction and valence bands, often referred to as the Seto model [30]. The lower valence band at the GB will repel holes from the GB region, and it is often suggested that this is a reason for the ineffectiveness of GB recombination. However, a positively charged GB will also attract electrons, and we find that the net effect is a performance decrease. Conversely, negative charge at the GB will yield a performance increase, but since negative-charged states in p-type material are not common, this scenario is considered unlikely.

The third type of alteration of the GB region in Fig. 5-10 is a change in the energy of the valence-band maximum, assuming at least initially that the conduction band remains flat. In Fig. 5-11, the standard solar cell parameters are plotted against the recombination

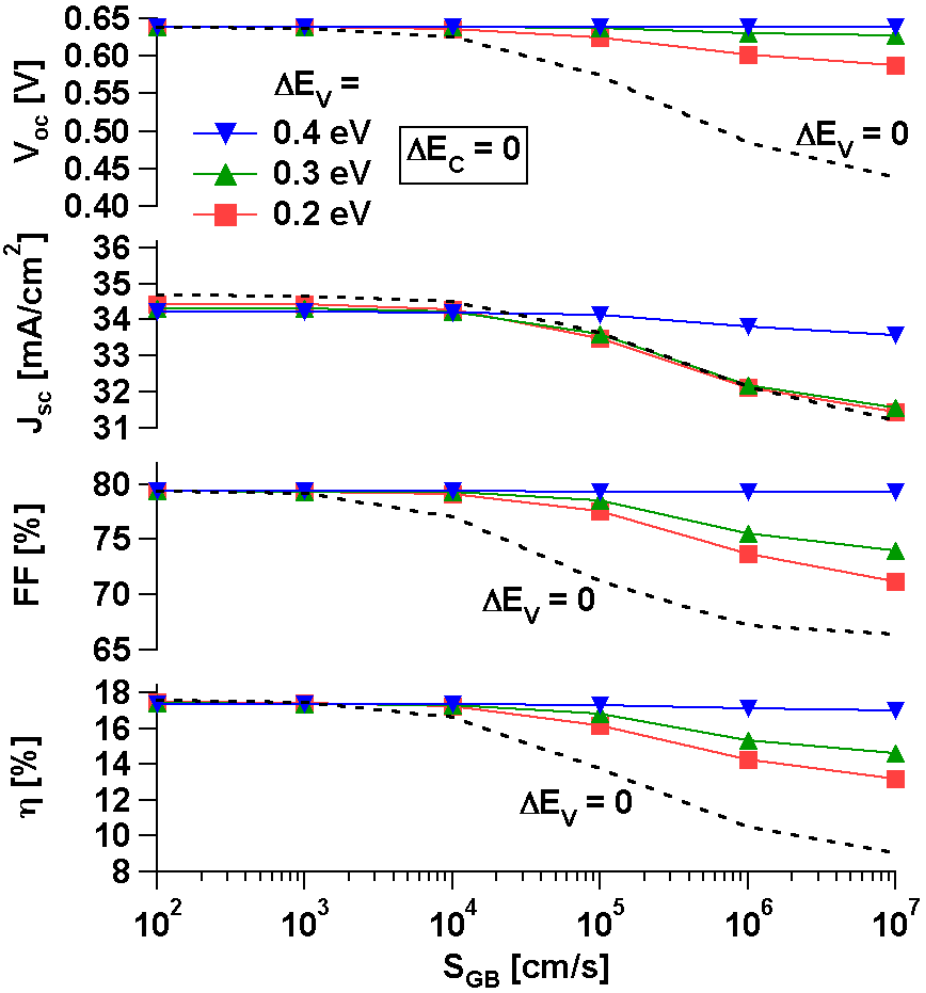

Figure 5-11. Recovery of CIGS GB losses with lower valence band ΔE_V.

velocity due to grain boundaries. The dashed line is the result without band alteration, and a GB recombination velocity that is varied over several orders of magnitude. Starting at about 10^4 cm/s, all the cell parameters show a decrease with increasing S_{GB}. If one lowers the valence band near the GB, keeping the conduction band flat, the holes are effectively shielded from GB recombination, and the parameters increase towards their values in the absence of GB recombination. Physically, this situation may be due to excess indium near the GB, which can result in an expanded band gap [31] and most likely affects the valence band. It is also consistent with the atomic-level calculations of Persson and Zunger [32], which predict a lowered valence band in the immediate vicinity of the GB. It is important to note, however, that the simulations cannot prove the validity of these physical models, but can only demonstrate that they are consistent with device performance.

REFERENCES

[1] S.S. Hegedus and W.N. Shafarman, "Thin-Film Solar Cells: Device Measurements and Analysis," Progress in Photovoltaics **12**, 155-176 (2004).

[2] X. Wu et.al., "16.5%-Efficient CdS/CdTe Polycrystalline Thin-Film Solar Cell," Proc. 17th European PVSEC, Munich (2001), pp 995-1000.

[3] J.R. Sites, "Quantification of Loss Mechanisms in Thin-Film Polycrystalline Solar Cells," Solar Energy Mat. and Solar Cells **75**, 243-251 (2003).

[4] S.-H. Wei, S.B Zhang, and A. Zunger, "Effects of Ga Addition to $CuInSe_2$ on its Electronic, Structural, and Defect Properties," Appl. Phys. Lett. **72**, 3199-3201 (1998).

[5] J.Hou, S.J. Fonash, and J. Kessler, "An Experimental and Computer Simulation Study of the Role of CdS in CIS-Type Solar Cells, Proc. 25th IEEE PVSC, Washington DC (1995), pp 961-964.

[6] I.L. Eisgruber, J.E. Granata, J.R. Sites, J. Hou, and J. Kessler, "Blue-Photon Modification of Nonstandard Barrier in $CuInSe_2$ Solar Cells," Solar Energy Mat. and Solar Cells **53**, 367-377 (1998).

[7] M.A. Contreras et. al., "High Efficiency $Cu(In,Ga)Se_2$-Based Solar Cells: Processing of Novel Absorber Structures," Proc. 24th IEEE PVSC, Hawaii (1994) pp 68-75.

[8] J.E. Granata, J.R. Sites,G. Contreras-Puente, and A.D. Compaan, "Effect of CdS Thickness of CdTe Quantum Efficiency," Proc 25th IEEE PVSC, Washington DC (1995), pp 853-856.

[9] J.F. Hiltner and J.R. Sites, "High-Resolution Laser Stepping Measurements on Polycrystalline Solar Cells," Proc. 16th European PV Solar Energy Conf., p.630 (2000).

[10] J.F. Hiltner and J.R. Sites, "Micron-Resolution Photocurrent of CdTe Solar Cells Using Multiple Wavelengths," Mat. Res. Soc. Proc. **668,** H9.8 (2001).

[11] S.D. Feldman, R.T. Collins, V. Kaydanov, and T.R. Ohno, "Effects of Cu in CdS/CdTe Solar Cells Studied with Patterned Doping and Spatially Resolved Luminescence," Appl. Phys. Lett. **85**, 1529-1531 (2004).

[12] O. Breitenstein, J.P Rakotoniaina, and M.H. Al Rifai, "Quantitative Evaluation of Shunts in Solar Cells by Lock-in Thermography," Prog. Photovolt: Res. Appl. **11**, 515-526 (2003).

[13] D. Shvydka, A.D. Compaan, and V.G. Karpov, "Nonlocal Response in CdTe Photovoltaics," J. Appl. Phys. **91**, 9059-9065 (2002).

[14] M. Contreras *et al*. "High Efficiency Cu(In,Ga)Se_2-Based Solar Sells: Processing of Novel Absorber Structures," Proc. 24th IEEE PVSC, Hawaii (1994), pp. 68-75.

[15] D. Tarrant and J.H. Ermer, "I-III-V Multinary Solar Cells Based on $CuInSe_2$," Proc. 23rd IEEE PVSC, (1993), pp. 372-378.

[16] K. Ramanathan *et al*. "High Efficiency Cu(In,Ga)Se_2 Thin-Film Solar Sells Without Intermediate Buffer Layers," Proc. 2nd World Photovoltaic Solar Energy Conference, Vienna (1998) pp. 477-481.

[17] J.T. Heath, J.D. Cohen, and W.S. Shafarman, "The Study of Bulk and Metastable Defects in Copper Indium Gallium Diselenide Thin Films Using Drive-Level Capacitance Profiling," J. Appl. Phys. **95**. 1000-1010 (2004).

[18] D.P. Halliday, M.D.G. Potter, D.S. Boyle, and K. Durose, "Photoluminescence Characterization of Ion-Implanted CdTe," Proc. Mater. Res. Soc. Symp. **668,** H1.8.1-6 (2001).

[19] D.H. Rose, F.S. Hasoon, R.G. Dhere, D.S. Abin, R.M. Ribelin, X.S. Li, Y. Mahathongdy, T.A. Gessert, and P. Sheldon, "Fabrication Procedures and Process Sensitivities for CdS/CdTe Solar Cells," Prog. Photovolt. **7**, 331-340 (1999).

[20] S.-H. Wei, Private Communication (2004).

[21] D.L. Bätzner, G. Agostinelli, A. Romeo, H. Zogg, and A.N. Tiwari, "Voltage Dependent Carrier Collection in CdTe Solar Cells," Proc. Mater. Res. Soc. Symp. **668,** H5.17.1-6 (2001).

[22] J.E. Phillips and M. Roy, "Resistive and Photoconductive Effects in Spectral Response Measurements," Proc. 20th IEEE PVSC (1988), pp. 1614-1617.

[23] J.R. Sites, H. Tavakolian, and R.A. Sasala, "Analysis of Apparent Quantum Efficiency," Solar Cells **29**, 39-48 (1990).

[24] W.N. Shafarman, R. Klenk, and B.E. McCandless, "Device and Material Characterization of Cu(In,Ga)Se_2 Solar Cells with Increasing Band Gap," J. Appl. Phys. **79**, 7324-7328 (1996).

[25] J. Malmström, J. Wennerberg, M. Bodegård, and L. Stolt, "Influence of Ga on the Current Transport in CdS/Cu(In,Ga)Se_2 Thin-Film Solar Cells," Proc. 17th European PVSEC, Munich (2001), pp.1265-1268.

[26] M. Turcu and U. Rau, "Fermi-Level Pinning at CdS/Cu(In,Ga)$(Se,S)_2$, Interfaces: Effect of Chalcopyrite Alloy Composition," J. Phys. Chem. Solids **64**, 1591-1595 (2003).

[27] T. Minemoto, Y. Hashimoto, W. Shams-Kolahi, T. Satoh, T. Negami, H. Takakura, and Y. Hamagawa, Solar Energy Mat. Solar Cells **75**, 121-128 (2003).

[28] M. Topič, F. Smole, and J. Furlan, "Band-Gap Engineering in CdS/Cu(In,Ga)Se_2 Solar Cells," J. Appl. Phys. **79**, 8537-8540 (1996).

[29] O. Lundberg, M. Bodegård, J. Malmström, and L. Stolt, "Influence of the Cu(In,Ga)Se_2 Thickness and Ga Grading on Solar Cell Performance," Prog. Photovoltaics **11**, 77-88 (2003).

[30] J.Y.W. Seto, "The Electrical Properties of Polycrystalline Silicon Films," J. Appl. Phys. **46**, 5247 (1975).

[31] S.B. Zhang, S.-H. Wei, and A. Zunger, "Defect Physics of the $CuInSe_2$ Chalcopyrite Semiconductor," Phys. Rev. **B57**, 9642-9656 (1998).

[32] C. Persson and A. Zunger, "Anomolous Grain Boundary Physics in Polycrystalline $CuInSe_2$: The Existence of a Hole Barrier," Phys. Rev. Lett. **91**, 266401-1-4 (2004).

7. RECOMMENDATIONS

The primary recommendation is that the thin-film-polycrystalline community continue to utilize, and in fact expand, its device-physics strategies. These strategies should consist of a healthy mix of measurement, analysis, and simulation. A mature approach to device physics can be extremely valuable for bringing experimental results together, for serving as a reality check on proposed explanations, and for assisting in the design of new experiments with systematic variations in key cell parameters. It is a natural part of a team approach to CdTe and CIGS research. Specific areas where device-physics should continue to be applied include:

(1) Effects of elevated-temperature stress and bias and illumination cycles. With CdTe and CIGS cells, this is both a scientific and a marketing issue. We need to understand the several modes of performance change and to demonstrate whether such change can be kept within reasonable bounds.

(2) Thin absorbers. There are clear advantages in materials utilization and fabrication speed if CdTe and CIGS absorbers can be made thinner, but there are indications of possible performance loss. The goals should be to determine the specific nature of the loss and determine whether it is an inherent problem.

(3) Non-uniformities. There are several categories of non-uniformities that are common in CIGS and CdTe these cells, and there are several useful experimental techniques, including our LBIC. The models for these categories need further development, and they need to be applied to many specific cells.

(4) Grain boundaries. The grain boundaries of CIGS and CdTe cells can have an impact on cell performance. We need to better determine the general electrical nature of these grain boundaries and to better quantify their impact.

(5) Secondary barriers within the primary junction and at the back contact. Diode barriers are classic device-physics problems, and much of the general framework for assessing them is in place. As with the other areas, there is the practical issue of determining their specific nature and their magnitude.

8. COMMUNICATIONS

8.1. Publications

1. P.K. Johnson, A.O. Pudov, J.R. Sites, K. Ramanathan, F.S. Hasoon, and D.E. Tarrant, "Comparison of Trap States Bewteen CIGSS/CdS/ZnO and Cd PE CIGSS/ZnO Cells," European PVSEC **17**, 1035-1038 (2001).

2. A.O. Pudov, J.R. Sites, and T. Nakada, "Performance and Loss Analyses of High-Efficiency Chemical Bath Deposition (CBD)-ZnS/Cu($In_{1-x}Ga_x$)Se_2 Thin-Film Solar Cells," Jpn. J. Appl. Phys. **41**, L672-674 (2002).

3. J.R. Sites, "Quantification of Losses in Thin-Film Polycrystalline Solar Cells," Solar Energy Mat. and Solar Cells **74**, 243-251 (2002).

4. P.K. Johnson, A.O Pudov, J.R. Sites, K. Ramanathan, F.S. Hasoon, and D. Tarrant, "Interface Properties of CIGS(S)/Buffer Layers Formed by the Cd-Partial Electrolyte Process," IEEE PVSC **29**, 764-767 (2002).

5. A.O. Pudov, M. Gloeckler, S.H. Demtsu, J.R. Sites, K.L. Barth, R.A. Enzenroth, and W.S. Sampath, " Effect of Back-Contact Copper Concentration on CdTe Cell Operation," IEEE PVSC **29**, 760-763 (2002).

6. A.L. Fahrenbruch, "Comparison of Experimental Data and AMPS Modeling of the Effects of CdS Layer Thickness on the CdS/CdTe Solar Cell," IEEE PVSC **29**, 583-586 (2002).

7. K. Ramanathan, F.S. Hasoon, S. Smith, H. Al-thani, J. Allleman, H.S. Ullal, J. Keane, P.K. Johnson, and J.R. Sites, "Properties of Cd and Zn Partial Electrolyte Treated CIGS Solar Cells," IEEE PVSC **29** 523-526, (2002).

8. J.R. Sites, "Quantification of Loss Mechanisms in Thin-Film Polycrystalline Solar Cells," Solar Energy Mat. Solar Cells **75**, 243-251 (2003).

9. B.E. McCandless and J.R. Sites, "Cadmium Telluride Solar Cells", in *Handbook of Photovoltaic Science and Engineering,* A. Luque and S.S. Hegedus, Ed., John Wiley, pp. 617-662 (2003).

10. K. Ramanathan, F.S. Hasoon, S. Smith, D.L. Young, M.A. Contreras, P. Johnson, A.O. Pudov, and J.R. Sites, "Surface Treatment of $CuInGaSe_2$ Thin Films and its Effect on the Photovoltaic Properties of Solar Cells," J. Phys. Chem. Solids **64**, 1495-1498 (2003).

11. T. Potlog, L. Ghimpu, P. Gashin, A. Pudov, T. Nagle, and J.R. Sites "Influence of Annealing in Different Chlorides on the Photovoltaic Parameters of CdS/CdTe Solar Cells," Solar Energy Mat. Solar Cells **80**, 327-334 (2003).

12. M. Gloeckler, C. Jenkins, and J.R. Sites, "Explanation of Light/Dark Superposition Failure in CIGS Solar Cells," Proc. Mat. Res. Soc **763**, 231-236 (2003).

13. C. Jenkins et. al., "CdTe Back Contact: Response to Copper Addition and Out-Diffusion," National Center for Photovoltaics Review Proceedings (2003).

14. M. Gloeckler, A.L Fahrenbruch, and J.R. Sites, "Numerical modeling of CIGS and CdTe Solar Cells: Setting the Baseline," Proc. 3rd World Conf. on Photovoltaic Energy Conversion, 491-494 (2003).

15. M.A. Contreras, T. Nakada, M. Hongo, A.O. Pudov, and J. R. Sites, "ZnO/ZnS(O,OH)/Cu(In,Ga)Se_2/Mo Solar Cell with 18.6% Efficiency," Proc. 3rd World Conf. on Photovoltaic Energy Conversion, 570-573 (2003).

16. K. Durose et. al (including J.R. Sites)., "Physical Characteristics of Thin-Film Solar Cells," Progress in Photovoltaics **12**, 177-217 (2004)..

17. M. Gloeckler and J.R. Sites, "Apparent Quantum Efficiency Effects in CdTe Solar Cells," J. Appl. Phys. **95**, 4438-4445 (2004).

18. C.R Corwine, A.O. Pudov, M. Gloeckler, S.H. Demtsu, and J.R. Sites, "Copper Inclusion and Migration from the Back Contact of CdTe Solar Cells," Solar Energy Mat. and Solar Cells **82**, 481-489 (2004).

19. A.O. Pudov, M.A. Contreras, T. Nakada, H.-W. Schock, and J.R. Sites, "CIGS J-V Distortions in the Absence of Blue Photons," Thin Solid Films, in press.

20. M. Gloeckler and J.R. Sites, "Efficiency Limitations for Wide-Band-Gap Chalcopyrite Solar Cells," Thin Solid Films, in press.

21. P.K. Johnson, J.R. Sites, J.T. Heath, D. Cohen, and K. Ramanathan, "Defect Differences Between Selenized and Evaporated CIGS(S) Solar Cells," submitted to Progress in Photovoltaics.

22. D.S. Albin, T.J. Berniard, S.H. Demtsu, and T.J. McMahon, "Improved CdS/CdTe Solar Cell Stability Through Mitigation of Edge Shunts," submitted to J. Appl. Physics.

23. A.O. Pudov, F.S. Hasoon, A. Kanevce, H. Al-Thani, and J.R. Sites, "Secondary Barriers in CdS/$CuIn_{1-x}Ga_xSe_2$ Solar Cells," submitted to J. Appl. Physics.

8.2. Presentations

1. J.R. Sites, “Solar Electricity,” Colorado State Physics Colloquium, September 2001.
2. P.K. Johnson, “Trap State Comparison,” Munich, October 2001.
3. J.R. Sites, “Solar Electricity,” Broomfield Rotary Club, February 2002.
4. J.R. Sites, “Capacitance Basics,” CdTe Team Meeting, Cocoa FL, March 2002.
5. A.O. Pudov, “Variations in Back-Contact Copper,” CdTe Team Meeting, Cocoa FL, March 2002.
6. A.L. Fahrenbruch, “Modeling CdTe Cells,” CdTe Team Meeting, Cocoa FL, March 2002.
7. M. Goleckler, “Micro-nonuniformities with LBIC,” CdTe Team Meeting, Cocoa FL, March 2002.
8. P.K. Johnson, “CdS vs Cd-PE," CIS Team Meeting, New Orleans, May 2002.
9. J.R. Sites, “Surface Treatment of $CuInGaSe_2$,” International Conference on Ternary and Multinary Compounds,” Paris, October 2002.
10. T.J. Nagle, “Micro-nonuniformity ,” CdTe Team Meeting, Golden, October 2002.
11. S.H. Demtsu, “Electrical Characterization of FSI Cells,” CdTe Team Meeting, Golden, October 2002.
12. A.L. Fahrenbruch, “Modeling of FSI Cells,” CdTe Team Meeting, Oct. 2002.
13. J.R. Sites, “Back-Contact Copper,” CdTe Team Meeting, Golden, Nov. 2002.
14. J.R. Sites, “Losses in Thin-Film Polycrystalline Cells,” Aoyama Gakuin Univ., Tokyo, November 2002.
15. A.L. Fahrenbruch, “Practical Guide to Simulation,” Modeling Workshop, Golden, January 2003.
16. M. Goleckler, “Superposition Failure in CIGS,” Modeling Workshop, Golden, January 2003.
17. J.R. Sites, “Thin-Film Polycrystalline Solar Cells,” Univ. Wyoming Colloquium, Larimie, February 2003.
18. C.R. Jenkins, “Copper Migration in CdTe”, NCPV Review, Denver, March 2003.
19. M. Gloeckler, “Superposition Failure in CIGS,” Materials Res. Soc. Symposium, San Francisco, April 2003.
20. M. Gloeckler, “Baselines for CIGS and CdTe Simulation,” Third World Conf. On PV Energy Conversion,” Tokyo, May 2003.
21. J.R. Sites, “Losses in Thin-Film Polycrystalline Cells,” Univ. Kyoto, May 2003.
22. C.R. Jenkins, “PL from Single-Crystal CdTe,” Rocky Mountain AVS, Denver, June 2003.
23. J.R. Sites, “Micro-nonuniformities,” CdTe Team Meeting, Golden, July 2003.
24. S.H. Demtsu, “CdTe Stress Changes,” CdTe Team Meeting, Golden, July 2003.
25. J.R. Sites, “Third Level Metrics,” CdTe Team Meeting, Golden, July 2003.
26. M. Gloeckler, “Demystifying Apparent Quantum Efficiency,” CdTe Team Meeting, Golden, July 2003.
27. J.R. Sites, “Thin-Film Solar Cells,” CSU Mechanical Engr., September 2003.
28. J.R. Sites, “Solar Cell Loss Analysis,” University of Nevada, Las Vegas, September, 2003.

29. M. Gloeckler, "Solar-Cell Simulation," University of Delaware, October 2003.
30. J. R. Sites, "Solar Cell Loss Analysis," University of Toledo, October 2003.
31. A.O. Pudov, "J-V Distortions in CIGS Cells," NREL, October 2003.
32. J.R. Sites, "Thin-Film Solar Cells," University of Denver, October 2003.
33. P.K. Johnson, "Defects in Evaporated and Selenized CIGS Cells," CIS Team Meeting, Cocoa, FL, November 2003.
34. A.O. Pudov, "J-V Distortions in CIGS Cells," CIS Team Meeting, Cocoa, FL, November 2003.
35. M. Gloeckler, "Effects of CIGS Band Offset", CIS Team Meeting, Cocoa, FL, November 2003.
36. J.R. Sites, "CIGS Junction Alternatives," CIS Team Meeting, Cocoa, FL, November 2003.
37. A.L Fahrenbruch, "Simulation of CdTe Back Contacts," CdTe Team Meeting, Toledo, February 2004.
38. T.J. Nagle, "CdTe Non-uniformities by LBIC," CdTe Team Meeting, Toledo, February 2004.
39. C.R. Corwine, "Photoluminescence of Crystalline CdTe," CdTe Team Meeting, Toledo, February 2004.
40. J.R. Sites, "Third-Level Metrics," CdTe Team Meeting, Toledo, February 2004.
41. M. Gloeckler, "CIGS Efficiency Limitations," European Materials Research Society (E-MRS), Strasbourg, May 2004.
42. A.O. Pudov, "CIGS J-V Distortions," E-MRS, Strasbourg, May 2004.
43. J.R. Sites, "Chalcogenide Solar Cells: Choosing the Window," E-MRS, Strasbourg, May 2004.
44. M. Gloeckler, "CdTe Apparent Quantum Efficiency," 19th European Photovoltaic Conference, Paris, June 2004.
45. S.H. Demtsu, "CdTe Stability Issues," Renewable Energy Academic Program, Cocoa, FL, August 2004.
46. M. Gloeckler, "Band-gap Grading in CIGS Cells," 14th International Conference on Ternary and Multinary Materials, Denver, September 2004.
47. A.L. Fahrenbruch, "Simulation of Thin CdTe," NCPV Review, Denver, October 2004.
48. J.R. Sites, "When are Simulations Helpful?" NCPV Review, Denver, October 2004.
49. T.J. Nagle, "Local J-V from LBIC," NCPV Review, Denver, October 2004.

8.3. Graduate Degrees

1. Caroline Jenkins (M.S., May 2002) Coursework/Research Project.

2. Markus Gloeckler (MS, December 2002), Thesis: "Numerical Modeling of CIGS Solar Cells: Definition of the Baseline and Explanation of Superposition Failure."

3. Pamela Johnson (PhD, May 2003), Thesis: "The Effect of Trapping Defects on CIGS Solar-Cell Performance".

4. Samuel Demtsu (MS, May 2003), Coursework/Research Project.

5. Timothy Nagle (MS, May 2003), Coursework/Research Project.

6. Jun Pan (MS, May 2004), Coursework/Research Project

7. Alan Davies (MS, May 2004), Coursework/Research Project

8.4. Additional Reports

Caroline Jenkins	Unisun Characteriztion	December 2001
Markus Gloeckler	FSEC Micro-nonuniformities	March 2002
Caroline Jenkins	EPV ZIS/CIS Characterization	May 2002
Samuel Demtsu	First Solar CdTe Charaterization	July 2002
Caroline Jenkins	EcoSolar CdTe Characterization	July 2002
Alex Pudov	High-efficiency ZnS/CIGS Cells	December 2002
Alan Fahrenbruch	What is Lifetime?	February 2003
Demtsu/Nagle	FSI/USF/UT Stress Tests	June 2003
Caroline Jenkins	Surface Preparation Effect on CdTe PL	June 2003
Alex Pudov	J-V-T on NREL CdS/CIGS Cells	June 2003
Markus Gloeckler	AMPS/SCAPS Comparison	June 2003
Samuel Demtsu	First Solar I-Cells	July 2003
Alan Davies	NREL ZnS/CIGS Cells	August 2003
Timothy Nagle	GSE CIGS on Foil: LBIC with Bias	October 2003
Timothy Nagle	Astropower Bight Spots on Ref. Cell	December 2003
Jun Pan	ISET CIGS and Molybdenum Foil	December 2003
Samuel Demtsu	First Solar I-Cells	January 2004
Kanevce/Pudov	NREL CIS J-V Under Red Light	March 2004
Markus Gloeckler	Collection Efficiency Pitfalls (to IEC)	April 2004
Gloeckler/Sites	$J_L(V)$: Good vs Fair CIGS Cells (to IEC)	July 2004
Ana Kanevce	NREL ZnS/CIGS Cells	August 2004
Jun Pan	Thin CdTe Simulations (to Toledo)	August 2004
Timothy Nagle	NREL CdTe LBIC Features	August 2004